STUDY OF THE SELECTIVE GROWTH OF THIN FILMS: EFFECTS OF A THIRD SPECIES IN ATOMIC LAYER DEPOSITION

A Thesis

Presented to the Faculty of the Graduate School

of Cornell University

in Partial Fulfillment of the Requirements for the Degree of

Master of Science

by

Taewon Suh

January 2017

ABSTRACT

Electronic devices and their constituents have scaled down over generations for higher performance, lower power consumption, and continuation of Moore's Law. As their nanostructures emerge in forms of 3D and more complex geometries, precise control is highly desirable when constructing integrated circuits in semiconductors. Thus, deposition of thin films on dielectrics without affecting metal regions and vice versa is favorable. Atomic layer deposition (ALD) has exhibited the ability to grow uniform and conformal films of controlled thickness and composition. With these advantages, ALD is a good candidate to achieve selective area deposition for future semiconductor devices. Previous research has been conducted using solution-phase site-blocking layers and/or photolithography for patterning. In this thesis, a process that is more compatible with existing manufacturing lines in industry is studied.

In an ALD cycle, we introduced a third species called a co-adsorbate which is proposed to bind to one surface but not the other, disrupting deposition of the metal precursor via competitive and/or reversible adsorption. Ethanedithiol (EDT) was used as one of the co-adsorbate species for intrinsic difference in affinities of thiol functional group towards SiO_2 and Cu surfaces. Under an appropriate partial pressure of EDT, chemisorption of a metal precursor, tetrakis(ethylmethylamido)zirconium (TEMAZ), was completely blocked on Cu without disturbing growth on the other substrate, for one set of conditions. X-ray photoelectron spectroscopy confirmed the presence of sulfur only on Cu, indicating that EDT acted as a good site-blocking layer on the metal surface. We used another co-adsorbate, triethylamine (TEA), to study its role in an adsorption reversing and/or site-blocking process. TEA has an analogous chemical structure as the ligand of TEMAZ. In excess of TEA, the extent of dissociation of TEMAZ on a surface will likely be minimized leading to desorption, or reversed adsorption, of

TEMAZ. At a high partial pressure of TEA, growth inhibition on the two surfaces was observed while at a lower pressure of TEA, selective deposition of Zr was achieved. Experimental conditions for the latter were then used for a 1½ cycle study. Not only the type of the co-adsorbate, but also the effect of the partial pressure ratio of TEA to TEMAZ and substrate temperatures were also investigated. Three substrate temperatures of 120, 150, and 180 °C along with no, low, and high partial pressure of TEA were studied. Generally, less deposition was observed at higher temperatures, while the presence of TEA completely suppressed, if at all, chemisorption on Cu.

Reduction of the reactivity of a metal precursor by adduct formation may also help achieve selective area deposition. Trimethylaluminum (TMA) and water is the most well-studied system in the ALD community, and TMA is known for its high reactivity due to an empty p orbital of the Al atom. Preliminary density functional theory (DFT) calculations of the effect of formation of a Lewis acid-base complex are reported in this thesis in collaboration with the DiStasio group.

BIOGRAPHICAL SKETCH

Taewon Suh was born in Daegu, South Korea on January 8th, 1992. For a broader perspective in a bigger world, he decided to study abroad in the U.S. He attended King's high school in Seattle where he found interest in mathematics, chemistry, and physics. Upon graduation in 2010, he chose to study chemical engineering, a major that combined all three subjects, at University of Minnesota – Twin Cities with the God Global Excellence Scholarship. As an undergraduate researcher, he worked with Professor Chris Macosko on functionalization of epoxy with graphene loading and layer-by-layer deposition of polymers on PET. In 2014, He received bachelor's degree in chemical engineering with a minor in chemistry.

For further pursuit of surface science, Taewon joined the Engstrom Research Group (ERG) at Cornell University. Under the guidance of Professor James R. Engstrom, he studied various approaches to achieve film growth on selective areas using atomic layer deposition for two and a half years. After receiving Masters of Science degree in chemical engineering, he plans to continue his investigation of selective-area deposition with Professor Engstrom during his PhD degree.

ACKNOWLEDGEMENTS

First of all, I would like to thank Professor James R. Engstrom for his acute guidance during my pursuit of the MS degree. Without his ideas for new projects, suggestions for different experiments, and critiques on results, I would not have made it this far. His distinguished insight and incomparable experience with surface science and vacuum studies have guided me in a successful path. Not only have I gained fundamental knowledge but also, I have personally grown in persistence and ability while solving intellectual challenges I met along the way.

In addition, I would like to thank my colleagues in the ERG, Wenyu Zhang, Rambert Nahm, Jiun-Ruey Chen, and Hugh Bullen, for not only teaching me how to run and maintain a vacuum system, but also making research more enjoyable with countless funny moments. I especially want to show my gratitude to Jiun-Ruey for making me actively think about ways to solve problems and helping me learn about various components of the chamber faster.

I want to express gratitude to my collaborators, Professor Robert A. DiStasio Jr. and his students, Ka Un Lao and Jonathan Wong. Their experience with quantum chemistry and density functional theory has guided me to explore a different field of surface science. Based on simulation results, I will conduct corresponding experiments to compare theoretical and experimental outcome.

TABLE OF CONTENTS

Abstract ……..iii

Biological Sketch ……....v

Acknowledgements.…….……..vi

1. Introduction

1.1 Industry 1

1.2 Atomic Layer Deposition..... 3

1.3 Selective Area ALD 6

1.3.1 Self-assembled Monolayers with Photolithography 7

1.3.2 Competitive/Reversible Chemisorption..... 8

1.3.3 Adduct Formation 13

2. Experimental Setup..... 14

2.1 Chamber Setup..... 14

2.2 Microreactor Setup..... 21

2.3 X-ray Photoelectron Spectroscopy 22

2.4 Materials 25

2.5 Delivery System..... 26

3. Experiments 27

3.1 TEMAZ-TEA/EDT Co-adsorption Study..... 27

3.1.1 Sample Preparation 27

3.1.2 Microreactor Preparation 29

3.1.3 Half Cycle Study..... 31

3.1.4 1½ Cycle Study..... 35

3.1.5 XPS Analysis 38
3.2 Temperature-Partial Pressure Ratio Study 40
3.2.1 Sample Preparation 40
3.2.2 Experiments 40
3.3 Lewis Acid-Base Complex 42
4. Results and Discussions 42
4.1 Co-adsorption of TEMAZ and EDT/TEA 42
4.1.1 Effect of EDT 42
4.1.2 Effect of TEA 47
4.1.3 1½ Cycle Study 50
4.2 Effect of Substrate Temperature and Partial Pressure Ratio 53
4.2.1 Simulation Model (Matlab) 53
4.2.2 Effect of Temperature 57
4.2.3 Effect of Partial Pressure Ratio 57
4.3 Effect of Adduct Formation 60
5. Conclusions 65

LIST OF FIGURES

Figure 1-1 Moore's Law. The number of transistors in different processors as a function of time …….……2

Figure 1-2 Predicted surface coverage vs. exposure time at a fixed temperature, assuming Langmuiran Kinetics ……..4

Figure 1-3 Schematic representation of an ALD cycle. The first half cycle consists of pulse of the metal precursor and its purge. The second half cycle is for the co-reactant…..5

Figure 1-4 A schematic representation of an ALD process with the co-adsorbate species that is introduced during, and after the pulse of the metal precursor…….9

Figure 1-5 A schematic representation of mechanism involved in reversible chemisorption. The co-adsorbate (HL) in red may reverse the adsorption on one surface but not the other…….12

Figure 2-1 AutoCAD drawing of UHV chamber during (a) deposition and (b) surface analysis……...16

Figure 2-2 Temperature calibration curve as a function of heater power for various sample holders. Lines labeled SiO_2 and Cu represent actual substrate temperatures while the reference temperature is a measurement near the manipulator……18

Figure 2-3 AutoCAD drawing of the microreactor and its head…….…23

Figure 2-4 AutoCAD drawing of a section of the delivery line with a switching mechanism which can direct flows either to the microreactor or to the pump…….28

Figure 3-1 Exposure sequence for the high partial pressure EDT experiment……34

Figure 3-2 Exposure sequence for 1½ cycle experiment with the low partial pressure of TEA ……....37

Figure 3-3 A line scan on 4 in. Cu substrate along z-axis for 1½ cycle experiment without TEA (reported in section 3.1.4). Integrated intensity of Zr(3d) as a function of position……...…39

Figure 4-1 XP spectra of Zr(3d) for experiments with no, low, and high partial pressures of EDT on SiO_2 (left) and Cu (right) substrates…….44

Figure 4-2 XP spectra of S(2p) on Cu for the high and low EDT experiments……..45

Figure 4-3 XP spectra of Zr(3d) for experiments with no, low, and high partial pressures of TEA on SiO_2 (left) and Cu (right) substrates…….48

Figure 4-4 XP spectra of N(1s) on Cu for the no, low, and high TEA experiments……...49

Figure 4-5 XP spectra of Zr(3d) for 1½ experiments with no and low partial pressures of TEA on SiO_2 (left) and Cu (right) substrates…….51

Figure 4-6 Integrated intensities of Zr(3d) for ½ and 1½ cycle experiments with/without TEA on both SiO_2 and Cu substrates……..52

Figure 4-7 Surface coverage as a function of exposure time from the simulation model. The red vertical line is when the surface coverage reaches its steady state for the no co-adsorbate case……...…56

Figure 4-8 Atomic density of Zr on SiO_2 for no, low, and high TEA experiments at various temperatures……...…58

Figure 4-9 Atomic density of Zr on Cu for no, low, and high TEA experiments at various temperatures……...59

Figure 4-10 DFT calculations of energy change during adduct formation of TMA with NH_3 and H_2O and methane elimination reactions. Energies are calculated at infinitely separated reactants, starting complex (S.C.) of methane elimination, transition state (T.S.), ending complex (E.C.), and products……...…..61

Figure 4-11 DFT calculations of energy change during methane elimination reaction between TMA/SiH_3OH and TMA-NH_3/SiH_3OH. TMA/H2O shown in dashed line for

reference Energies are calculated at infinitely separated reactants, starting complex (S.C.) of methane elimination, transition state (T.S.), ending complex (E.C.), and products……...63

LIST OF TABLES

Table 3-1. Exposure sequence for ½ cycle ALD with TEMAZ without co-adsorbate……...32

Table 3-2. Exposure sequence for ½ cycle ALD with TEMAZ with the high partial pressure of EDT……...33

Table 3-3. Exposure sequence for 1½ cycle ALD with TEMAZ/O_2 with the low partial pressure of TEA…….36

Table 3-4. (a) Exposure sequence for ½ cycle ALD with TEMAZ with high low partial pressure of TEA and (b) vapor pressures of the reactants and their ratios in "low" and "high" cases…….41

Table 4-1. Parameters/equations used in the simple model to generate the two curves in Figure 4-7……...55

1. Introduction

1.1 Industry

Gordon Moore, a co-founder of Intel Corporation observed in 1965 that the number of transistors on integrated circuits per unit area doubled every year to a year and a half [1]. This is known as the famous Moore's Law and continuation of this trend is represented in Figure 1-1. It has been an important objective semiconductor companies have tried to achieve thus has become a driving force for the industry. In addition, as consumers desired smaller portable electronic devices, a need for denser array of transistors became inevitable. How was the industry able to satisfy these customers' needs for the past 50 years? What is the future plan or possible alternative route when critics judge that the Moore's Law has come to a stop?

The industry continues its search for next-generation techniques with particular characteristics that can overcome prevailing challenges. Since modern electronic devices already possess components of nm-scale, an advanced process is desired to have the same level of control over material thickness. The semiconductor industry would like this improved process to have not only precise control of film thickness, but also the ability to deposit films on 3D features of devices. In addition, compatibility with current manufacturing process in which gas-phase techniques are mostly employed can be a plus when integrating the developed technique to an existing one. It is also essential for prospective techniques to be capable of selective area deposition, only coating on surfaces of interest without disrupting nature of others. Atomic layer deposition (ALD) meets some of these requirements and has potential to achieve the others. Further research is necessary to accomplish selective area deposition using ALD which is the main focus of this thesis. But first, fundamental mechanism of ALD will be reviewed and we will study two methods of how it can be incorporated into developing a process that can achieve

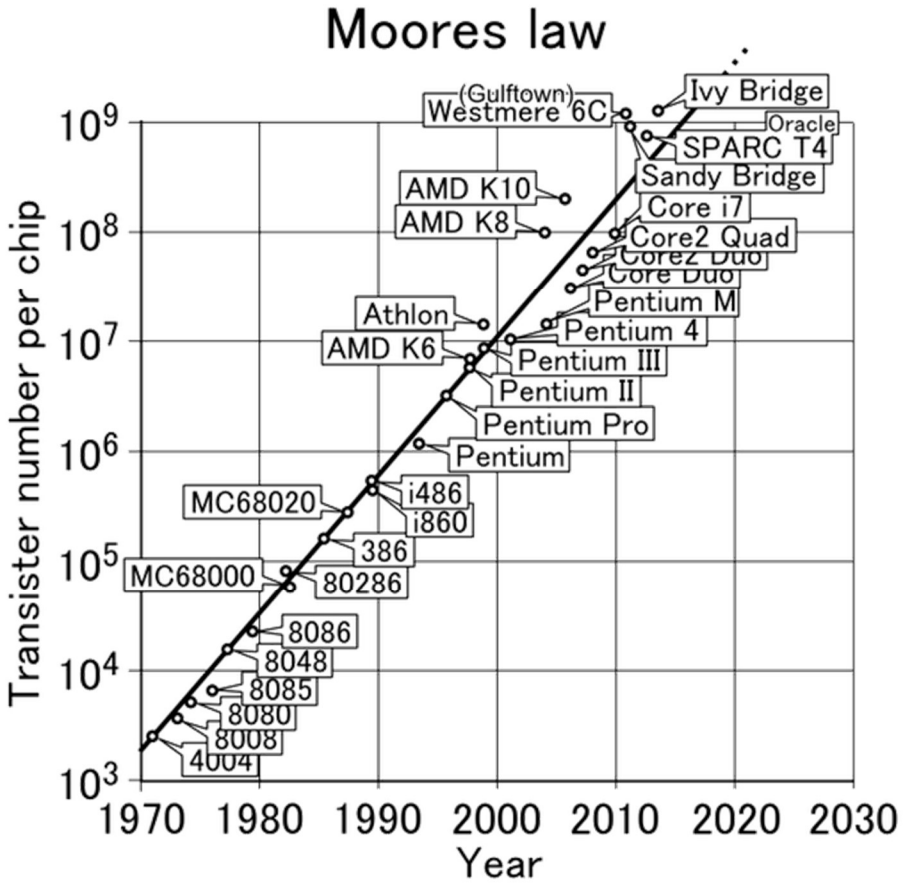

Figure 1-1 Moore's Law. The number of transistors in different processors as a function of time

selective area growth: introduction of a co-adsorbate species and formation of a Lewis acid-base complex.

1.2 Atomic Layer Deposition

ALD has emerged as a potential approach capable of matching the rapid rate of downscaling of semiconductor devices. The fundamental property of ALD that draws much attention from industry is the self-limiting nature of chemistry involved, indicating that no further reaction takes place once all active sites have been reacted. This key feature brings about two major advantages of ALD: precise control of thickness of deposited film and conformal deposition [2]. ALD is sequential, binary reaction in which a precursor is introduced to the surface at a time and saturates the surface with a monolayer given sufficient exposure time. Figure 1-2 is a plot of surface coverage of a precursor as a function of exposure time, assuming first order Langmuirian kinetics. A monolayer coverage given enough exposure time is true for both reactants, thus ALD is known to possess a unique characteristic of self-limiting growth. A cycle of ALD consists of two half cycles, separated by purge steps to prevent any unwanted parasitic reactions in gas phase as seen in Figure 1-3. During the first half cycle, the substrate is exposed to an organometallic or metal organic precursor, referred to reactant A in this thesis. After a saturating dose of a metal precursor, a purge step takes place to get rid of unreacted gas-phase A molecules. In the second half cycle, a co-reactant, water or molecular oxygen in a typical ALD process for oxide films, is then introduced to the substrate [3]. Another purge of the reaction zone is conducted to prepare a co-reactant-free reaction zone before the next cycle of ALD.

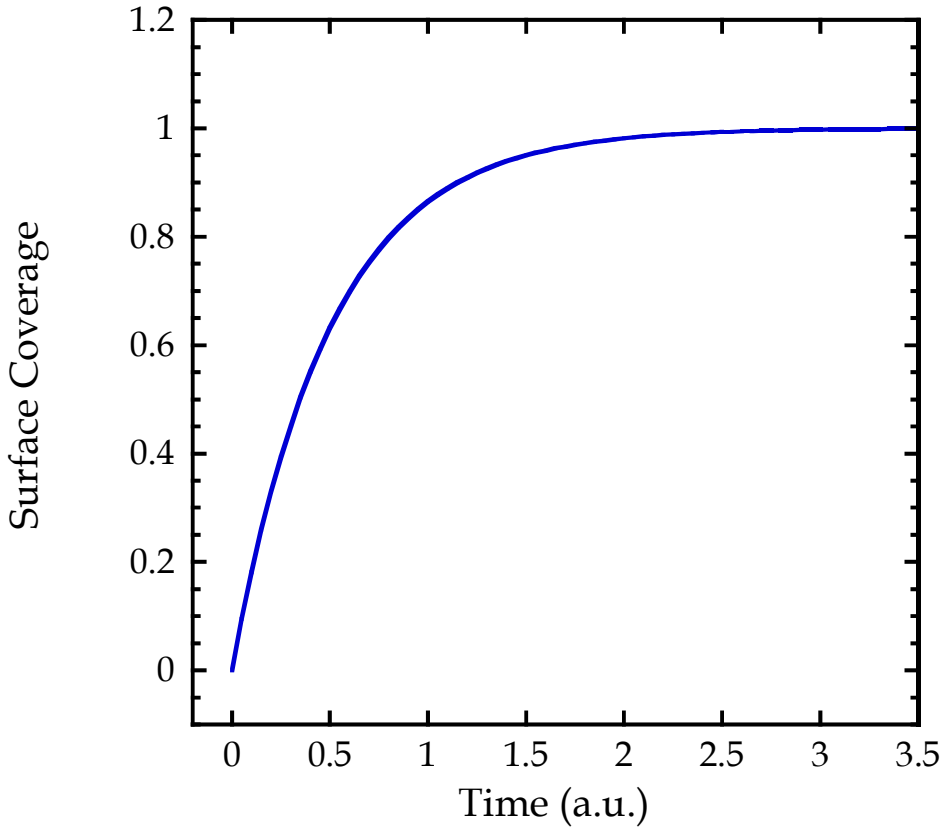

Figure 1-2 Predicted surface coverage vs. exposure time at a fixed temperature, assuming Langmuiran Kinetics

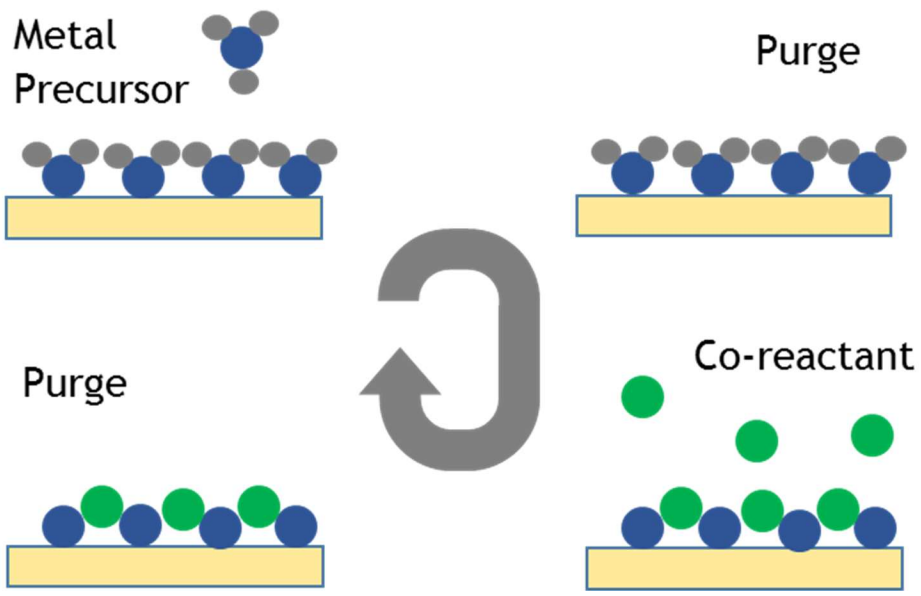

Figure 1-3 Schematic representation of an ALD cycle. The first half cycle consists of pulse of the metal precursor and its purge. The second half cycle is for the co-reactant

There are only a finite number of reaction sites in every step of an ALD cycle. Since both the metal precursor and co-reactant undergo self-terminating surface reactions, only a finite number of each species is deposited within a cycle [4]. Since the amount of film deposited depends on the number of cycles, not on the time of exposure to reactants, given sufficient exposure time, ALD processes are capable of precise control over thickness of grown film. In other thin-film deposition techniques such as chemical vapor deposition (CVD), thicker films grow wherever the higher flux of incoming precursors is. This is due to the absence of the self-limiting nature of the chemistry used in such process, in which the thickness of deposited film is time-dependent, not the number of cycle dependent. In an ALD process, transport properties of precursors can be neglected since only a monolayer of film will deposit within a cycle regardless of the precursor flux. In addition, ALD can conformally coat surfaces with complex features, a capability unique to ALD [5]. If sufficient time is allocated for precursor exposure, precursor molecules will ultimately reach every active site, even the ones located deep in trenches with high aspect ratios, depositing just one monolayer of film per cycle. This uniform film deposition in ALD processes allows films to grow while preserving the orientation of the previous layer.

1.3 Selective Area ALD

With the unique ability to control thickness of the deposited film and coat three-dimensional structures with complex shapes, ALD meets some fundamental characteristics required for future semiconductor devices. These fulfilled requirements include precise control of material thickness at the Å level, ability to coat features with high aspect ratios, and compatibility with current manufacturing process. To satisfy more needs of the future market, selective area ALD has been identified as one of the prospective research projects [6].

1.3.1 Self-Assembled Monolayers with Photolithography

To achieve selective area deposition, previous studies have modified substrates before ALD processes with self-assembled monolayers (SAMs). A typical SAM consists of a surface-active head group connected to an alkyl chain and a tail group. SAMs spontaneously chemisorb on the surface upon contact, forming a densely packed and stable two-dimensional system [7]. One of the crucial advantages in use of SAMs is that one can manipulate head or tail group and modify chemical reactivity of the surface as desired. Head groups can be chosen for selective deposition with their intrinsic difference in affinities towards different kinds of substrates while tail groups capable of blocking nucleation on top of SAMs may be preferred.

How did previous studies accomplish selective growth using SAMs? George Whitesides and his co-workers demonstrated modification of selective areas on substrates through microcontact printing of SAMs for various applications [8]–[10]. They were capable of patterning SAMs on different surfaces by the following procedure. As the first step in the preparation of SAMs, polydimethylsiloxane (PDMS) stamps are fabricated using conventional soft lithography. The stamp parts that protrude out towards the masters are dipped in a solution of SAMs before coming into contact with the substrate. Using this microcontact printing method, SAMs are patterned on the substrate, part of which exhibits different chemical and physical properties. Koide et al. have utilized this pretreatment of substrates to grow thin films of ZnO via selective area ALD [11]. The patterned SAMs of docosyltrichlorosilane (DTS) acted as a densely packed blocking layer, directing and defining location of ZnO thin films. The authors were able to selectively deposit 60 nm thick ZnO films on Si/SiO_2 substrates.

If the fully functional combination of SAMs and photolithography,capable of selective growth is available, why does the industry strive for a different technique for replacement? There

are several drawbacks with the use of SAMs. The primary shortcoming involves the quality of blocking layer produced by SAMs. Lim et al. observed that it takes at least a day of immersion of InP samples in octadecanethiol to form a complete 2D system of SAMs of high quality [12]. Similarly, McGuiness et al. discovered that the coverage of the same type of SAMs on GaAs reached only ~80% after ~ 12 hours [13]. Stacey Bent and her co-workers reported that submergence of substrates in solution of SAMs for ~40 hours would form a closely packed monolayer of the blocking agents [14]. These reported times on the order of days are not suited for sample preparation in typical industrial processes. In addition, SAMs are subject to dissociation at high temperatures which would likely result in defects and they may act as nucleation sites for incoming metal precursors. SAMs do not form a perfect 2D blocking layer on substrates with complex geometries since the layer of SAMs heavily relies on topography of the substrates as well. In a typical process involving SAMs, substrates are submerged into a solution of SAMs. In order to form a blocking layer with a minimized number of defects, precise control of concentration of SAMs is also required. In this thesis, different mechanisms involving gas-phase reactions, instead of solution-phase processing, are investigated as alternative approaches to achieve deposition on selective areas using ALD.

1.3.2 Competitive/Reversible Chemisorption

Instead of using SAMs, a third gas-phase species is introduced which is proposed to temporarily bind to one surface but not another, disrupting deposition of the metal precursor via competitive and/or reversible adsorption during an ALD process, the former shown in Figure 1-4. As the name suggests, competitive adsorption simply indicates cases in which the third “co-adsorbate” species competes against the metal precursor for active sites on the surface. There are

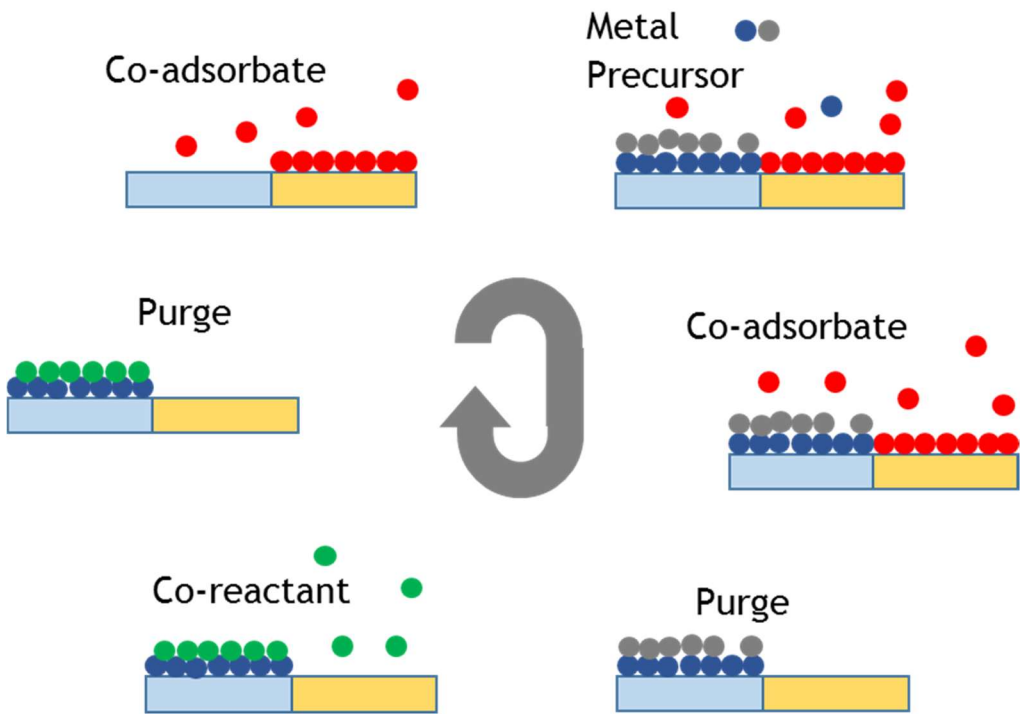

Figure 1-4 A schematic representation of an ALD process with the co-adsorbate species that is introduced during, and after the pulse of the metal precursor.

a few requirements for this mechanism to work along with a selective area ALD process. First, intrinsic difference in affinities towards different substrates must be considered prior to selecting the co-adsorbate molecule. This species has to adsorb more strongly to one surface but weakly (or preferably not at all) to another to construct a blocking layer only on one surface. Secondly, the desorption of the co-adsorbate should occur in subsequent steps to prevent any unwanted incorporation into the thin film. Bound co-adsorbate molecules preferably leave the surface during the purge step without participation in any reaction, leaving a clean surface behind. In addition, this co-adsorbate species does not chemically react with the metal precursor; rather, they compete to occupy surface active sites. And lastly, adsorbed blocking agents should be capable of suppressing growth or delaying nucleation of the metal precursor. The co-adsorbate molecules are introduced before, during, and after the dose of the metal precursor to ensure their dominant presence compared to their competitors.

In contrast to competitive adsorption, the fundamental concept of reversible adsorption is to minimize the extent of decomposition of the metal precursor. During the gas-surface reaction between a transition metal precursor and substrate, the precursor loses its ligand(s) ultimately forming a covalent bond with surface atoms and being integrated into the film. This process could be expressed in the following generic form:

$$2 \vdash \mathrm{X}^{*} + \mathrm{ML_x} \rightleftharpoons \vdash \mathrm{X} \cdots \mathrm{ML_x^{*}} + \vdash \mathrm{X}^{*} \rightarrow \vdash \mathrm{X} - \mathrm{ML_{x-1}^{*}} + \vdash \mathrm{X} - \mathrm{L}^{*}$$

where X indicates a metal substrate, a surface site in typical ALD process, M is for the metal precursor, L is the ligand, and * denotes a surface species. As shown in the equation, the metal precursor chemisorbs onto a metal surface and is ready to lose a ligand to form an actual covalent bond. Dissociation of the precursor on the metal surface is comparatively easy to reverse; however, too much dissociation may not guarantee reversibility. To prevent the reaction

from going beyond this point-of-no-return, maintaining the number of ligands in excess in the surroundings is essential to increase the yield of backwards reaction according to Le Chatelier's principle. A third species with similar chemical structure to the ligands of the metal precursor, if not identical, is used to shift the equilibrium in the reverse direction. A schematic diagram of the adsorption reversal process is shown in Figure 1-5. Just like in the situation of competitive adsorption, pre-, co-, and post-exposure of the third species are employed to provide excess ligands that may recombine with the adsorbed metal precursor to form the reactant species. In addition to the chemical structure of the third species, the intrinsic affinities of the metal precursor towards different substrates needs to be considered. Once the co-adsorbate species is present in excess, bound metal precursors are likely to maintain their ligands. What makes this ALD process capable of selective deposition is the intrinsic affinity of the metal precursor. Thus, further investigation is required to determine which transition metal precursor binds much stronger to substrates of interest and then select the third species that would make the process reversible.

What is the purpose of investigating an ALD process involving competitive or reversible adsorption? There are two main reasons: one is to discover the existence of a selectivity window, ranges of parameters in which selective growth is achieved, and the other is to find out when selectivity is lost. At low partial pressure of the co-adsorbate and high enough substrate temperature, film of precursor material is likely to grow on two substrates (dielectric and metal in this thesis). Less co-adsorbate present, less likely it disturbs deposition of the precursor, while higher substrate temperatures aid in overcoming energy barriers of dissociative chemisorption. Deposition on both substrates at these conditions is likely to occur due to minimal effect of the blocking layer and/or reversible agents. Due to inherent difference in characteristics of the two

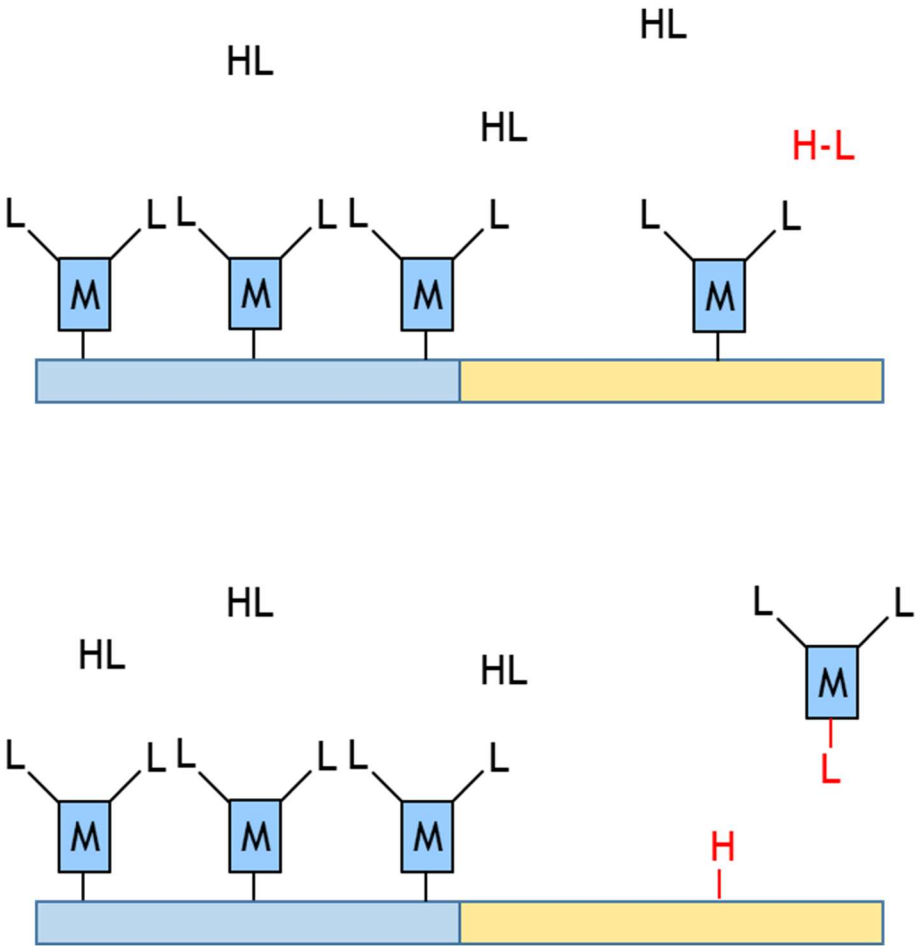

Figure 1-5 A schematic representation of mechanism involved in reversible chemisorption. The co-adsorbate (HL) in red may reverse the adsorption on one surface but not the other.

substrates, the behavior of film growth on the two substrates will likely vary at different experimental conditions. It is inevitable that there is a point where deposition on the two substrates starts to behave differently. The purpose of this study with co-adsorbate molecule is to identify such ranges of partial pressures of the co-adsorbate and temperatures in which film grows on one substrate but not on the other.

The second objective of the study is to find the most promising system of precursors for multiple cycles and when this system eventually fails. Thickness of films deposited within current manufacture lines ranges from several nm to hundreds of nm or even up to an order of μm, indicating a high number of cycles required to produce films of such thickness. A focus of the study will be to discover a combination of precursors that are best suited for multiple ALD cycles and find out how the mechanism involved in achieving selective area deposition depends on process conditions (i.e. substrate temperature, partial pressure of co-adsorbate). Growing films of multiple layers on selective area inherently imposes a risk of losing selectivity at certain point. Examining the fundamental mechanism behind the loss of selectivity (i.e. oxidation of a metal surface during co-reactant pulse which may result in possible nucleation sites) will suggest methods to prevent films from growing on both substrates by changing certain parameters.

1.3.3 Adduct Formation

As the most well-studied chemistry among thermal ALD processes; trimethylaluminum (TMA)/water is very promising in aspect of film growth that numerous companies in the semiconductor industry use this system to test their newly built ALD tools. If selective growth could be achieved with this process that is capable of growing film on basically any surface, if not all, it will be quite a discovery to the ALD community. Instead of using the co-adsorbate

species as the growth inhibition layer or reaction-reversing agent, a Lewis base will be used for study of selective area ALD of TMA. The LUMO of TMA (equivalent to p-orbital of aluminum) grants TMA its high reactivity and readily accepts a pair of electrons, making it a strong Lewis acid. Once acid/base molecules come to proximity, the Lewis base will donate a pair of electrons to the empty p-orbital of aluminum, reducing its high reactivity to some degree. Depending on how much the reactivity is reduced, the TMA-based Lewis acid-base complex may still be reactive enough to deposit on one surface but weakened too much for deposition on the other. Manipulating the reactivity of TMA via adduct formation is possible because TMA readily forms an adduct with a Lewis base such as ammonia without an activation energy barrier [15]. Preliminary density functional theory (DFT) calculations of various candidates for the Lewis base are conducted. Molecules centered around nitrogen vs. oxygen atoms are studied as well as the effect of the structure of ligands bound to the central atom (electron donating vs. withdrawing) on adduct formation. More detailed computational study of selective area deposition of TMA by adduct formation are investigated in collaboration with the DiStasio research group, Cornell University.

2. Experimental Setup

2.1 Chamber Setup

All experiments regarding selective area ALD investigated in this thesis were conducted in an ultrahigh vacuum (UHV) chamber. Detailed description of the chamber is reported in a previous journal article published by the Engstrom research group [16]. In this thesis, only the components of the system and their functions that are most relevant to experiments/analysis of selective area ALD are described.

The custom-designed UHV chamber can be subdivided into four sections in large: loadlock, microreactor, analysis chamber, and central chamber. The positions of the sample during deposition and analysis are different, as shown in Figure 2-1. The sample travels between the central and analysis chambers under UHV by the sample manipulator (Thermionics SMR-3, Thermionic Northwest, Port Townsend, WA). The manipulator allows the sample to be translated along three axes and be rotated about two axes. The three axes are defined as x, y, and z while the two directions of rotation are polar (in/out of the plane of the sample with the central vertical line as the axis of rotation) and azimuthal (within the plane of the sample). Movements along x and z axes and polar and azimuthal rotations are regulated by a computer-assisted step-motor controller. In order to prevent any leak during rotational motions, a differential seal is incorporated with the sample manipulator. A differential seal is created by layers of varying vacuum levels. For this specific sample manipulator, a higher vacuum is created by an ion pump (Ionpak 200, Perkin-Elmer Vacuum Products, Waltham, MA), capable of reaching UHV, while a lower one is generated by a mechanical rotary pump, typically producing 10^{-2} or 10^{-3} Torr. Having the higher level of vacuum surrounded by the lower one assists in reducing the pressure rise that would occur without pumping.

Samples of different substrates are attached to the manipulator via a sample holder; a holder grasps a sample(s) and is clipped onto the manipulator. A sample holder consists of two molybdenum platens; the back platen has shallow recess on which a sample sits and the front platen has a lip along the parameter which restricts movements of the samples between the two platens. Experiments described in this thesis were carried out using two different, but very similar in design, sample holders. One holds a circular four-inch wafer (with either SiO_2 or Cu films on top) while the other one simultaneously holds two rectangular substrates (SiO_2 and Cu),

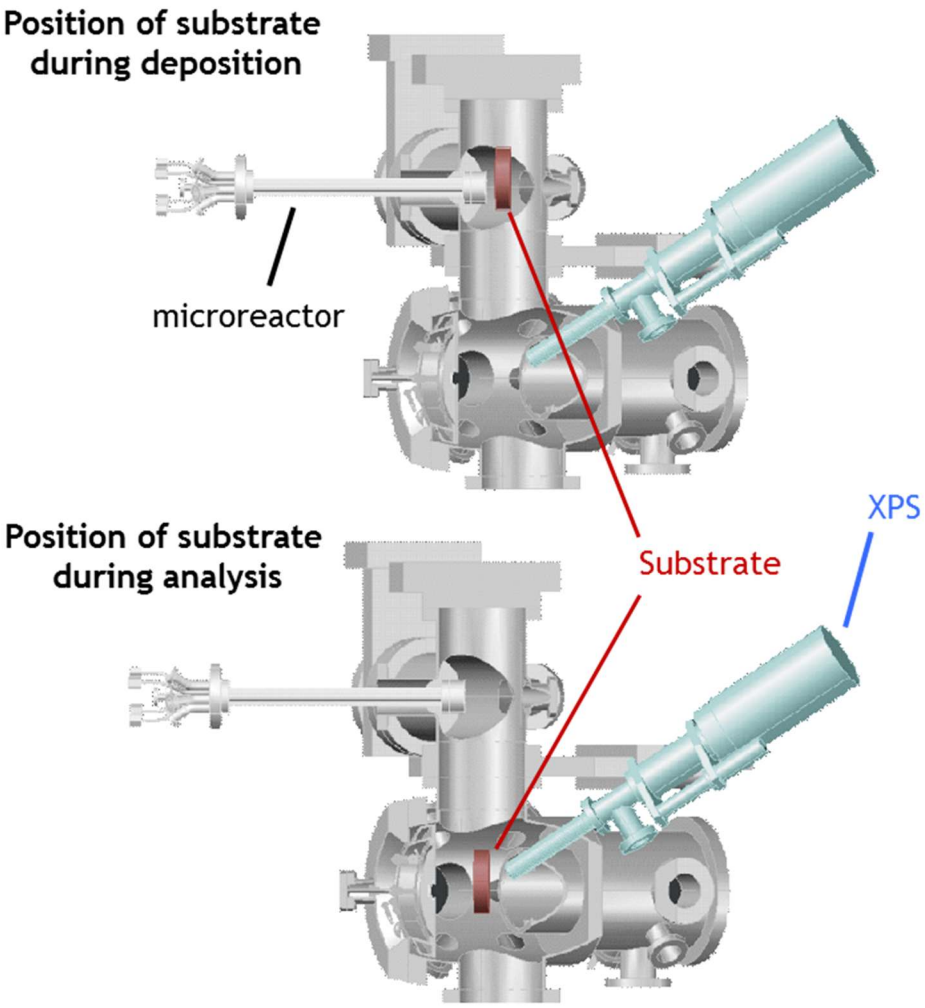

Figure 2-1 AutoCAD drawing of UHV chamber during (a) deposition and (b) surface analysis.

1.2 in by 0.4 in each. Thermal ALD processes require substrates at elevated temperatures; experiments in this thesis were conducted at substrate temperatures ranging from 120 °C to 180 °C. Hollow space in the back platen near the center is designed to expose the sample directly to radiative heating from the sample manipulator. The manipulator is equipped with heating element consisting of pyrolytic boron nitride, a typical type of heating element in many UHV chambers. Due to limited space for temperature measurement during an exposure, calibration of the substrate temperature is performed before experiments. A junction of chromel and alumel (thermocouple type K) is attached onto each substrate (Cu and SiO_2) using ceramic adhesive. Temperatures of the substrate surfaces, and a reference temperature measured near the manipulator were recorded as a function of the heater output, represented in percentage. Thermocouple readings for the two-slit sample holder and 4 in wafer holder along with the reference temperature are plotted as a function of heater power in Figure 2-2. Controlling the applied heater power and knowing the corresponding reference temperature for every experiment allow accurate approximation of the actual substrate temperature.

Samples are introduced to the chamber by clipping the sample holder onto fingers of the manipulator. Before venting the upper stage of the system (loadlock and central chamber), this section is isolated from the rest of the chamber (analysis chamber and microreactor) by corresponding gate valves. Once the loadlock and central chamber are vented with high purity nitrogen, one would insert the sample holder wearing a lab coat and gloves to avoid any contamination of the chamber wall from contact with skin oil. When the sample holder is mounted onto the manipulator and secured attachment between the holder and fingers are ensured, chamber walls are thoroughly wiped with isopropylalcohol (IPA) to minimize contamination. The process of loading samples is complete when the turbo molecular pump

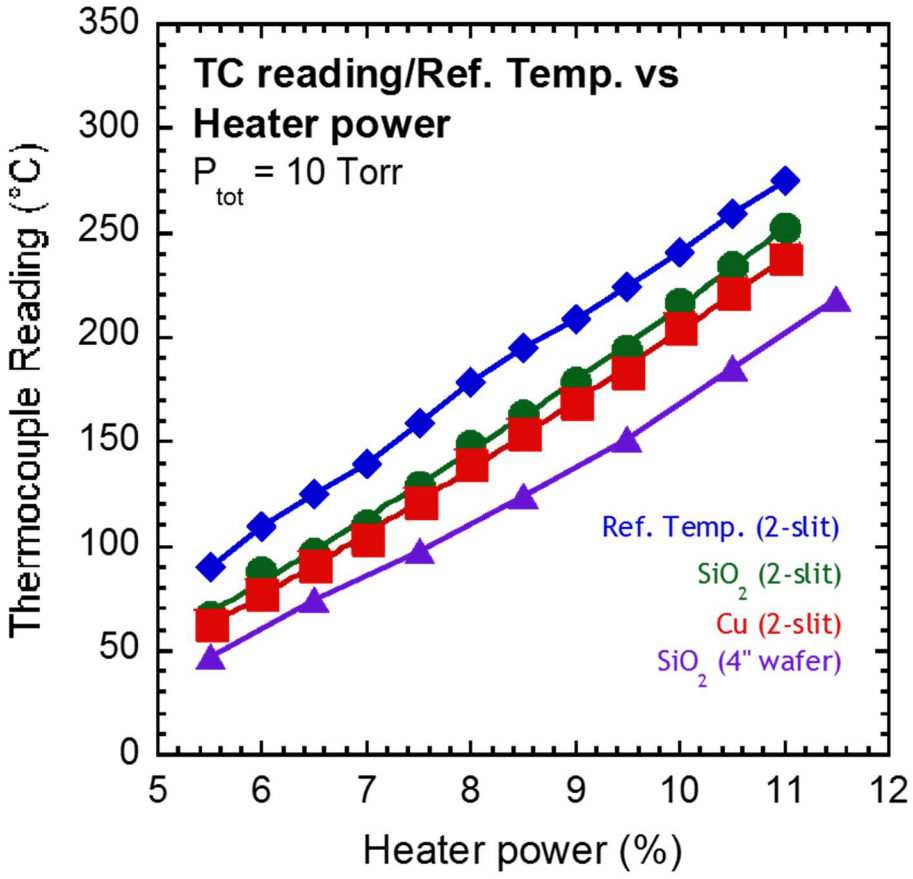

Figure 2-2 Temperature calibration curve as a function of heater power for various sample holders. Lines labeled SiO_2 and Cu represent actual substrate temperatures while the reference temperature is a measurement near the manipulator

attached to loadlock (Pfeiffer TMU 071 P) pumps down the vented chambers. When medium vacuum (~ 1.0 x 10^{-6} Torr) is measured by an ion gauge in the loadlock, samples/central chamber are ready to be set up for experiments.

The central chamber serves as a bridge between other sections of the system. It can be isolated from or connected to loadlock, microreactor, and analysis chamber by opening/closing corresponding gate valves in between. As mentioned above, the central chamber has several functions in operation of the system. The central chamber can be open to loadlock for sample loading or to the analysis chamber for transfer of samples down to the lower stage for post-characterization of deposited film. The most important purpose of the central chamber, however, is that it is where experiments are carried out. Before an experiment, the microreacor approaches and gets close enough to the sample holder in the central chamber. No mechanical seal between the head of the microreactor and the holder is made for confinement of the reaction zone. Nonetheless, a source of inert nitrogen gas, or curtain gas, is connected to the central chamber such that continuous flow of nitrogen flowing outside-in acts as a barrier to inhibit escape of reactants and introduction of contaminants during experiments. Details regarding set up of the microreactor will be discussed comprehensively later. After experiments at low vacuum (~10 Torr), samples are transferred down to the analysis chamber for *in situ* X-ray photoelectron spectroscopy (XPS). For this *in vacuo* transfer to occur, the pressure difference in the central volume (10 Torr) and analysis chamber (UHV) needs to be alleviated first. There is a bypass valve that connects the central and ante chamber. The ante chamber is stationed next to analysis chamber and contains a shutter through which a beam of precursors passes. Since the ante chamber is used for other experiments, details regarding are omitted in this thesis. As the bypass valve is slowly opened, the ante turbomolecular pump (Pfeiffer TPU 261 PC) expels any residual

gas species from the system. Once the foreline pressure of the ante chamber no longer increases, the pressure of the central chamber is low enough for connection to the main chamber for post-experiment surface analysis.

All of surface characterization and other analysis are done in the analysis chamber. It has several incorporated tools capable of quadrupole mass spectrometry (QMS), ion scattering spectroscopy (ISS), and XPS. QMS (Hiden 3F/EPIC QMS, Hiden Analytical, Warrington, UK) is used to analyze and quantify the ion signal for a range of mass to charge ratio (1~300) inside the chamber. QMS is used in He leak test to locate a source of leak within the system by detecting m/z of 4 and monitoring oxygen/water level for potential leaks. In addition, before experiments with the microreactor, beams of reactants, both metal precursor and co-adsorbate species, were made to identify and confirm characteristic signals unique to respective reactants.

Additional equipment is attached to the analysis chamber for analysis: concentric hemispherical analyzer (CHA), ion gun, and x-ray source. Both ISS and XPS use the same analyzer, CHA (SPHERA Energy Analyzer 125, Omicron Nanotechnology), to receive scattered ions or photoelectron/Auger electrons. As indicated by the name, the analyzer has two concentric hemispheres to which voltages are applied to make one negatively charged and the other positive. Ions/electrons/atoms enter through one side of the gap between the hemispheres and the detector lies on the other side to receive filtered species. Thin film deposited using selective area ALD reported in this thesis were not characterized with ISS; however, the ion gun was used to sputter the adventitious layer of carbon from gold standard samples. Sputter etch pretreatment of surfaces employed a beam of Ar^+ ions with energy of 3 keV for five to ten minutes.

It is essential to minimize the level of oxygen, water, and other possible impurities in the system for surface-sensitive analysis and deposition of thin films within a confined reactions

zone. Filaments in surface-sensitive analysis tools are exposed to risk of burning out in existence of oxidizing molecules. Presence of oxygen and water at high level in proximity of the reaction zone may result in CVD-like growth: co-exposure of a metal precursor and co-reactant. How do we keep the number of these unwanted reactions as small as possible? Attaining UHV with oxygen/water free environment is fundamental in study of surface science. During pump down, all the gate valves are open to have the entire system pumped by four turbomolecular pumps (main, ante, source, and loadlock), supported up by seven mechanical rotary pumps. Once the pressure of the chamber reaches medium to high vacuum, electronics and their cables are removed from the system for a bakeout. Two heating jackets (metal pieces with integrated heating elements) surround the chamber and they are heated to ~100 °C for evaporation of water molecules from the chamber wall. After the bakeout procedure for 24 to 36 hours, the pressure of the chamber is typically on the order of 10^{-9} Torr. Electronics are reattached afterwards and their degassing is performed. Realignment of motors are conducted for possible misalignment in deposition/analysis positions of the sample manipulator. The chamber with minimized water level is now ready for experiments.

2.2 Microreactor Setup

Jiun-Ruey Chen, a senior graduate student of the group, and his co-workers designed a reactor, called “microreactor”, capable of confining reactants in a small region for deposition. The fundamental motivation for design and construction of the microreactor is to restrict exposure of precursors to a small area and isolate that area from contaminants in the surroundings. Chen simulated the reactor using computational fluid dynamics (CFD) for

evaluation of precursor confinement. Details regarding structure and mechanism of the simulation will be included in his dissertation.

The microreactor capable of creating a confined reaction zone has been constructed according to results of the simulation and its schematic diagram is shown in Figure 2-3. In the front/head of the microreactor, the centermost area is the reaction zone surrounded by two effluent grooves. Unreacted gas-phase reactants and other inert gases will exit the reaction zone through these effluent grooves. There are also electrical probes for continuity tests. The microreactor head is connected to central fluidic extension pieces which are required for the head to go through chamber components such as the microreactor gate valve, mounting port, etc. There are two effluent feedthroughs that connect the effluent grooves to a mechanical pump. There are three inlet feedthroughs overall. For earlier experiments with TEMAZ-TEA in section 3.1, only two of the three inlets are used, while for later experiments, all three inlets are used.

2.3 X-ray Photoelectron Spectroscopy

The most frequently used surface analysis technique in this thesis is XPS. X-rays are generated within the analysis chamber by an Omicron DAR 400 source (Omicron Nanotechnology USA, Eden Prairie, MN) which has Mg and Al anodes. When electrons from a filament bombard either anode, X-rays with a known photon energy pass through an Al window which screens stray electrons. When the X-ray encounters film/substrate of interest, electrons of surface atoms are excited and some of them may escape with sufficient energy and detected by the analyzer. As previously described, the analyzer screens and quantifies electrons of specific kinetic energy. Since the photon energy produced by an anode ($h\nu$), the work function of the material (Φ), and the kinetic energy of emitted electrons measured by the analyzer (KE) are

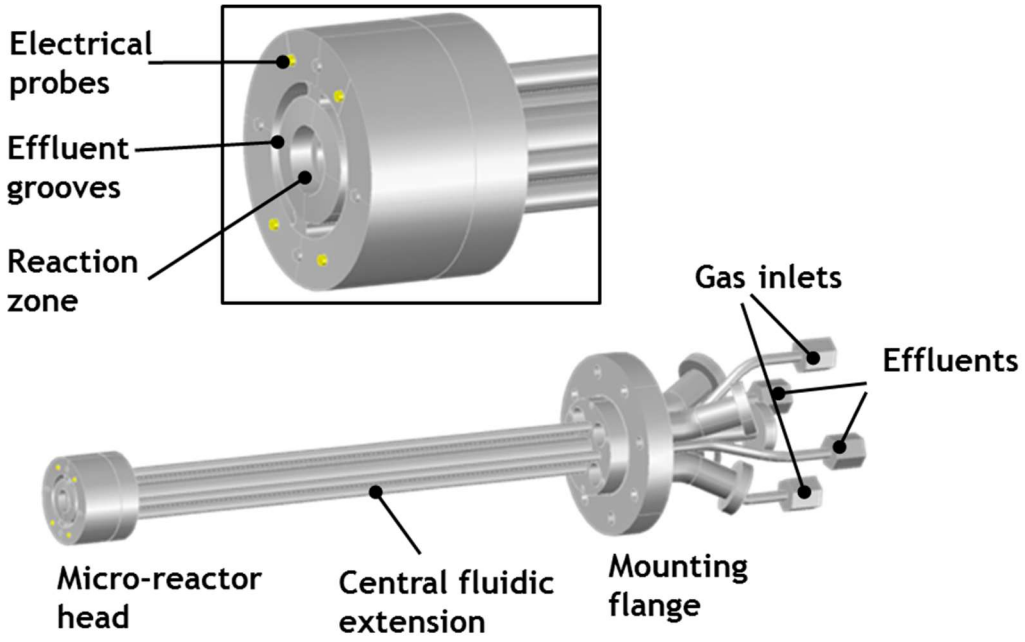

Courtesy: Jiun-Ruey Chen

Figure 2-3 AutoCAD drawing of the microreactor and its head.

known, the binding energy of each electron before excitation can be determined by the following equation:

$$BE = h\nu - KE - \Phi$$

Each element has unique binding energies of its core level electrons. Therefore, XPS allows identification of elements in film/substrate and their composition and relative amounts of existing elements can be quantified [17]. The binding energy for a core level electron, however, may vary depending on different oxidation states or bound environments by several eV's. This "chemical shift" gives additional information about valence state of elements such as the degree of oxidation of a transition metal from the organometallic precursor.

XPS is a surface-sensitive technique for electrons cannot travel over a certain distance, known as inelastic mean free path (λ) without losing its kinetic energy in a collision. In solids, λ is typically within the order of magnitude of 1 nm. Most signals in a XP spectra are from top ~10 nm of the film/substrate since electrons from atoms buried deeper than 10 nm are attenuated. For identification of elements, binding energies of peaks are compared to known values of corresponding elements. In some cases, there may be binding energy shift of several eV other than chemical shift. One possible cause of the shift is static surface charging and the magnitude of the shift varies sample to sample. To correct for the discrepancy in binding energy when comparing with tabulated values, elements like C, Si, or Cu are used. "Adventitious carbon" is carbon from the air or existing hydrocarbons in the UHV chamber. C (1s) peak is known to be 284.7±0.2 eV for aliphatic C so once the same peak is analyzed for a sample, the difference can be calculated and applied to correct for the binding energy shift [18]. Elemental Si ($2p_{3/2}$) peak at 99.8 eV or elemental Cu ($2p_{3/2}$) peak at 934.7 eV from underlying substrates can also be applied for binding energy correction [19], [20].

There are several steps in the analysis of XP spectra. First, the background needs to be determined for accurate measurement of peaks above. The background intensity is removed by the method developed by Shirley which makes the background proportional to the peak area above by iteration [21]. Then curve fits composed of a mixture of 70% Gaussian and 30% Lorentzian formula are used to integrate areas under peaks. Depending on the orbital of a scanned element, ratio of peak areas with doublet features are pre-defined according to their respective degeneracies. Once the intensity of an element is measured, surface density of the same element can be quantified as well. XPS of a Au sample consisting of 2000Å Au | 100 Å Ta| SiO_2 was done prior to other experiments for comparative calculation of elemental surface densities. For example, quantification of Zr (3d) surface density requires several numbers: intensities of Zr and Au (measured), their photoionization cross sections (tabulated by Scofield [22]), their transmission functions (function of kinetic energy), mean free path of Au photoelectrons (known), and surface density of Au (known). Relative evaluation with the Au standard enables calculation of how much of each element is present in film/substrate and one can ultimately identify its relative chemical composition.

2.4 Materials

Three reactants used in study of selective area ALD consist of a metal precursor, co-reactant, and co-adsorbate. The transition metal precursor used in experiments of this thesis is tetrakis(ethylmethylamido) zirconium (IV) (TEMAZ), or $Zr[N(CH_2CH_3)]_4$ (99.99%, Air Liquide). Co-reactant used in experiments reported here is molecular oxygen of ultra high purity in gas phase originating directly from a cylinder (Airgas, NY). There are two co-adsorbate species reported here: triethylamine (TEA) and 1,2-ethanedithiol (EDT) (both chemicals ≥ 98.5%

(GC), Sigma-Aldrich Corp.). Except for oxygen, all other reactants are in liquid phase and they require special containers. These liquid phase reactants (TEMAZ, TEA, and EDT) are stored in individual bubblers, made of 316L stainless steel with electropolished interior surface. The purpose of this specific processed material for the containers is to prevent any unwanted chemical reactions between the precursors and walls of containers and minimize introduction of contaminants/oxygen. Organometallic precursors typically generate flame in presence of oxygen or water so it is crucial to keep atmospheric air away from them. In addition to choice of material for a bubbler, how a precursor is loaded onto one matters. Air Liquide was requested to store TEMAZ in a cleaned bubbler due to extra level of caution when dealing with these chemicals. For TEA and EDT, loading process happens inside a glove box in the Nanobiotechnology Center (NBTC) at Cornell University, to minimize internal level of oxygen and water. H_2O and O_2 content inside the glove box is less than 1 ppm with the rest filled with N_2.

2.5 Delivery System

The phase of the reactants indicates incapability of being delivered to the reaction zone in an appreciable amount. Therefore, an inert gas, called carrier gas, which does not participate in gas-surface reactions with substrates transport vapor-phase reactants from their sources to substrates of interest. He was used to carry TEMAZ while N_2 was used for the other reactants. During exposure of a precursor, a carrier gas from a cylinder goes through a mass flow controller (MFC) and approaches a bubbler at a specified mass flow rate in sccm. The inlet of a bubbler has a dip tube that extends to the bottom such that an incoming carrier gas has sufficient time to reach equilibrium with the reactant and acquire reactants in vapor phase for delivery. The number of reactants in a stream of carrier gas exiting the bubbler is proportional to their partial

pressure which are experimentally controlled by the temperature of a bath for the bubbler. Conditions such as temperatures and flow rates for each line is discussed in more detail in description of flow patterns in section 3.1.2. There are pneumatic three-way valves downstream of each bubbler. These valves have an inlet and two outlets such that they dictate the direction of a flow: either to a mechanical pump for exhaust or the microreactor for deposition. For example, during a purge step, the carrier gas for metal precursor will be directed straight to the pump and the flow exits the system without encountering the substrates. The pneumatic valves are controlled by a computer program called LabView. The program controls status of all the pneumatic valves such that when they can be open or closed and compressed air will flow or not flow accordingly. Three-way pneumatic valves, MFC's and other manual diaphragm valves are supported by each standing panel and a bubbler lies underneath. A schematic diagram of a panel containing these pneumatic valves is shown in Figure 2-4. Three of these panels stand on a platform which rests on four carriages connected to a rail. The carriages enable the panels to move parallel and along with the microreactor when it approaches the sample holder for an experiment. The mobile delivery system is used to investigate the effect of temperature and partial pressure ratio of co-adsorbate to precursor on selective area ALD in section 3.2.

3. Experiments

3.1 TEMAZ-TEA/EDT Co-adsorption Study

3.1.1 Sample Preparation

Two substrates used in experiments for study of selective area ALD are Cu and SiO_2. Cu samples are cut to appropriate size, either 4 in x 4 in or 1.2 in x 0.4 in, from 300 mm Si wafers

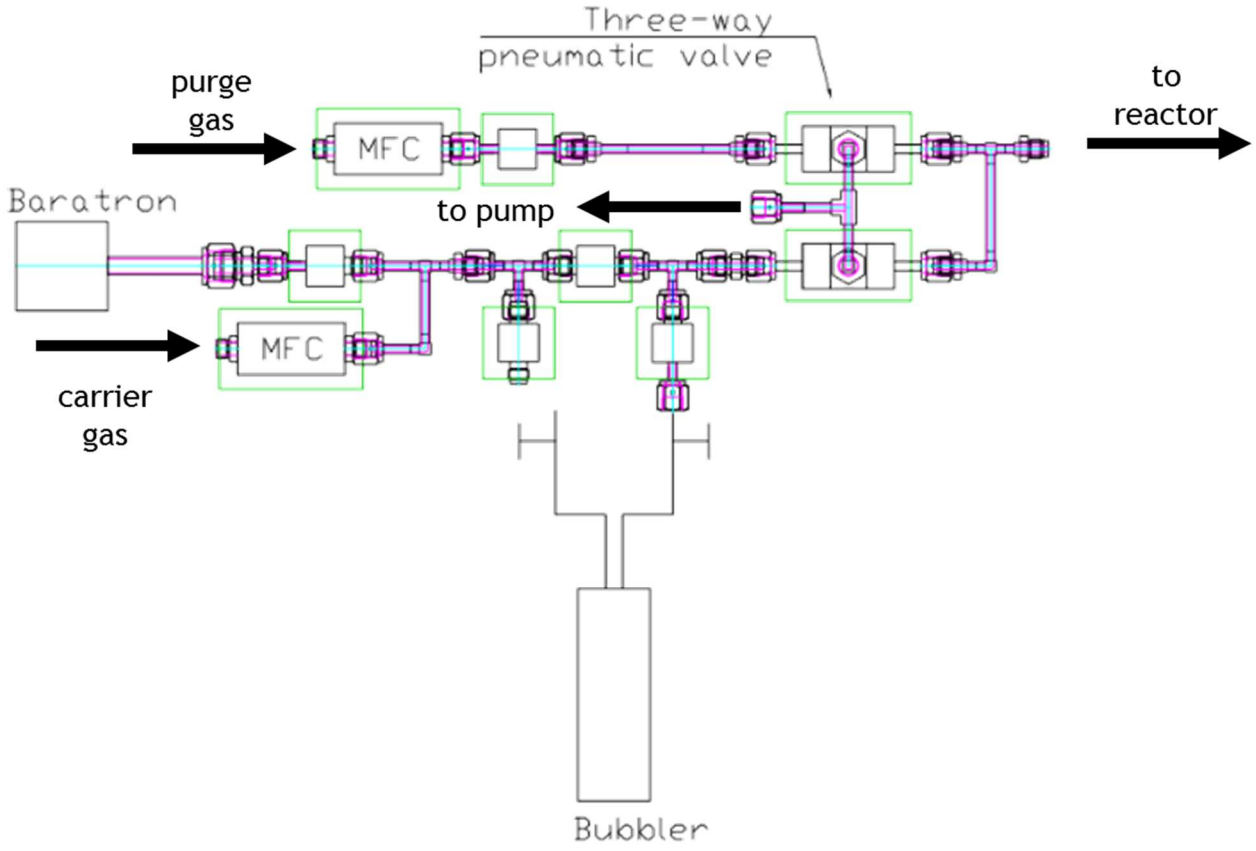

Figure 2-4 AutoCAD drawing of a section of the delivery line with a switching mechanism which can direct flows either to the microreactor or to the pump

provided by companies. A thick layer of Cu is deposited onto Ta on SiO_2 by PVD. The Cu layer is thick enough such that Ta and/or SiO_2 layer is not observed during surface analysis with XPS.

SiO_2 substrates are prepared using wet chemistry. A Si (100) wafer is cleaved to a desired size and taken to a clean room in Cornell Nanoscale Facility (CNF). Native SiO_2 is removed by submerging the sample in buffered oxide etch (BOE) (6:1) for 2 minutes. Hydrophobicity of the substrate surface is visually examined to determine the effectiveness at each step of the procedure. The BOE treatment generates hydrogen terminated Si, hydrophobic in nature. Droplets of distilled water molecules formed during rinse after the BOE treatment indicate a hydrophobic surface. Substrates are then immersed in a bath of nanostrip (90% H_2SO_4, 5% H_2SO_5, 5% H_2O, and <1% H_2O_2) heated to 75 °C for 15 minutes. Grown SiO_2 during this step is often called "chemical oxide" and this SiO_2 layer is hydroxyl group terminated with surface density of ~ 5 x 10^{-14} OH/cm^2 [23], [24]. Rinse after nanostrip treatment does not form droplets of water, rather, water disperses across the hydrophilic surface. The BOE/nanostrip steps are repeated to ensure a layer of OH-terminated SiO_2.

3.1.2 Microreactor Preparation

A prepared substrate (either Chem. Ox. or Cu) is loaded onto a 4 in-wafer holder. As described in section 2.1, the holder enclosing the substrate is attached onto the manipulator through the vented loadlock. When the upper stage of the chamber (central chamber and loadlock) is pumped down and its pressure reaches 10^{-6} Torr or lower, preparation for an experiment begins. The sample heater is turned on with heater power of 9.4% which generates substrate temperature of ~150 °C for the 4 in wafer holder. The loadlock gate valve is closed which makes the central chamber a stagnant volume, isolated from the system. A bellow-sealed

valve downstream of a MFC for the curtain gas (N_2) cylinder and upstream of the central chamber is opened to pressurize the central chamber to a higher pressure than that of the microreactor with the curtain gas leaking through the closed MFC. Once the gate valve to the microreactor is opened, the typical pressure inside the microreactor is ~ 2 Torr. Even though there is no pressure gauge in the central chamber, the pressure of the microreactor indicates that the pressure of the central chamber before opening the gate valve is higher than 2 Torr. This step is essential to eliminate possible backstreaming of pump oil from the microreactor mechanical pump (E2M30, Nandor Technologies, NY) to high vacuum in the central chamber. Once the central chamber and microreactor are safely pumped by the E2M30, 75 sccm of the curtain gas starts flowing. A throttle valve capable of PID control (MKS Instruments, MA) regulates openness of the valve such that the pressure of the microreactor is kept at a set point, 18 Torr in this set of experiments.

A linear motor stage is a platform on which the microreactor is mounted and allows it to travel in linear motion through a computer-assisted motor. Before an experiment, the microreactor typically travels 30,000,000 microsteps, equivalent to ~12 inches (1 μstep = 0.39 μinch). As the microreactor approaches the sample holder, continuity for four probes embedded in the head of the microreactor is checked along the way. Continuity for all four probes is critical in determining the orientation of the microreactor with respect to the holder and distance between them which is equivalent to the gap through which curtain gas flows. Three inlet feedthroughs and respective delivery lines (referred to Line A, B, and C for the precursor, co-reactant, and co-adsorbate) within the microreactor, are wrapped around and heated by tungsten wire in fiber glass.

A bubbler (SAFC Hitech, MA) that contains the metal precursor was heated up to and kept at 40 °C in a water bath (Thermo Fischer Scientific, NY), upstream of the inlet. A delivery line from the outlet of the bubbler to the feedthrough of the microreactor was also heated with a heating tape to remove any cold spot on which metal precursor may condense. The bubbler, delivery line, and line inside the microreactor were heated to 40 °C, 60 °C, and 80 °C, respectively, for effective delivery of the metal precursor to the reaction zone. Another bubbler (Strem Chemicals, MA) with the co-adsorbate species was in an ice bath or a bath of propylene glycol which was cooled down to -10 °C by a feedback-looped chiller depending on experiments to produce a desired partial pressure of the co-adsorbate and ratio of partial pressures between TEMAZ and TEA or EDT.

3.1.3 Half Cycle Study

Experiments with EDT included the two substrates and three different partial pressures of EDT: zero, low, and high. The first half-cycle of ALD of ZrO_x using TEMAZ/O_2 is done with and without the co-adsorbate to investigate the effect of its presence. The dosing sequence for the pristine deposition is shown in Table 3-1. The time of exposure was five minutes for each step and flowrate for each line was 10 sccm as noted. In experiments with the co-adsorbate species, EDT is introduced to substrates before, during, and after introduction of TEMAZ to ensure complete site-blocking reactions. The dosing sequence for the high partial pressure of EDT is represented in Table 3-2. Five minutes of each exposure step and 10 sccm of each gas species are used in each step again. An ice bath kept the EDT bubbler close to 0 °C which would produce a vapor pressure of 1.00 Torr according to the Antoine equation. The flow pattern for the high partial pressure EDT experiment is described in Figure 3-1. The green line representing the

Table 3-1. Exposure sequence for ½ cycle ALD with TEMAZ without co-adsorbate

Cycle	Step	Line A	Line C
1st half cycle	Pre-dose (5 min)	10 sccm He	10 sccm N_2
	Co-dose (5 min)	10 sccm TEMAZ (40 °C) | He	10 sccm N_2
	Post-dose (5 min)	10 sccm He	10 sccm N_2

Table 3-2. Exposure sequence for ½ cycle ALD with TEMAZ with the high partial pressure of EDT

Cycle	Step	Line A	Line C
1st half cycle	Pre-dose (5 min)	10 sccm He	10 sccm EDT (0 °C) | N_2
	Co-dose (5 min)	10 sccm TEMAZ (40 °C) | He	10 sccm EDT (0 °C) | N_2
	Post-dose (5 min)	10 sccm He	10 sccm EDT (0 °C) | N_2

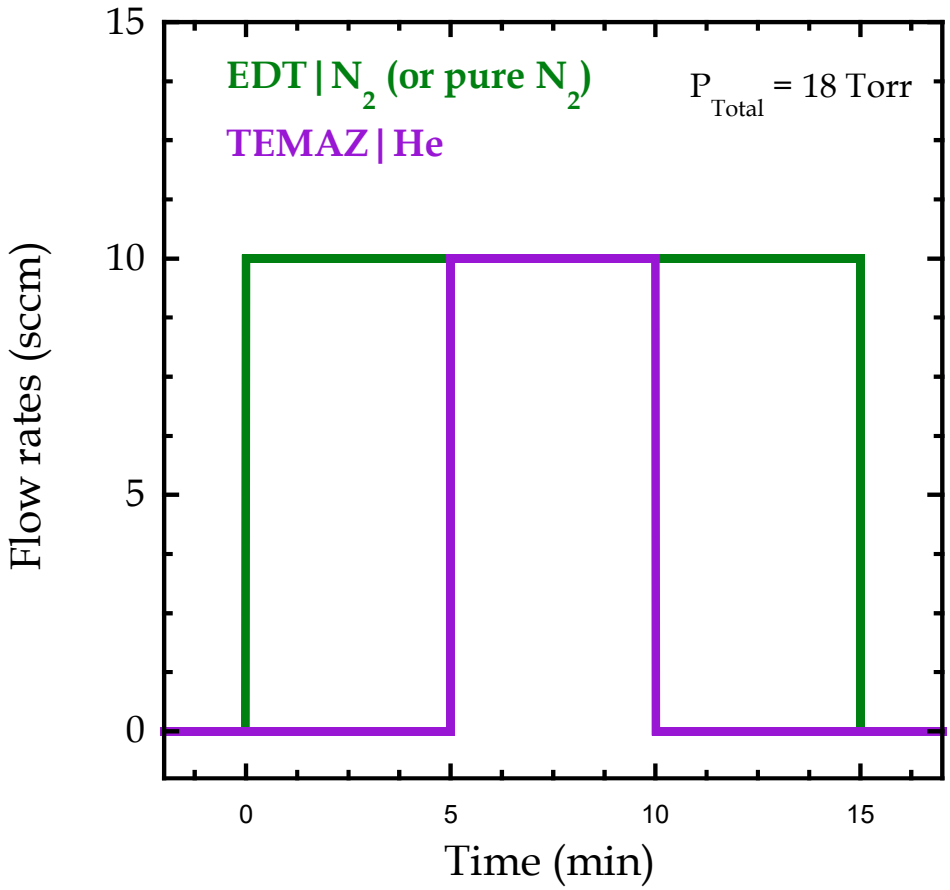

Figure 3-1 Exposure sequence for the high partial pressure EDT experiment.

stream of EDT | N_2 is introduced to substrates before the metal precursor. For the intermediate partial pressure of EDT, its effective partial pressure was decreased by factor of ~10 compared to the high-pressure case. The carrier gas of EDT was diluted by five times by mixing 2 sccm of EDT | N_2 with 8 sccm of N_2. In addition, the temperature of the bubbler was maintained at -10 °C in a bath of propylene glycol which produced vapor pressure of 0.45 Torr. The dosing sequence is identical to the flow pattern of the other EDT experiment except for the dilution ratio and bath temperature.

For the study of co-adsorption of TEA, three partial pressure ratios of TEMAZ to TEA are used as in the case of EDT: zero, low, and high. Both low and high partial pressures of TEA involved TEA at -10 °C, equivalent to 3.61 Torr. The only difference between them was the dilution ratio; the low concentration of TEA was generated by diluting 2 sccm of TEA | N_2 with 8 sccm of N_2 while entire 10 sccm of TEA | N_2 was used for the high case. Other parameters such as the flowrate and exposure time are identical to those of EDT experiments.

3.1.4 1½ Cycle Study

As discussed further in section 4.1.2, in the experiment with the low partial pressure of TEA, selective deposition of Zr was obtained: ~40% suppression on SiO_2 and complete inhibition of growth on Cu. The same experimental conditions including flowrates, bath temperatures, and dilution ratio of TEA stream were extended to a 1½ cycle experiment. In this 1½ cycles of ZrO_x ALD, exposure sequence is TEA-enclosed TEMAZ dose, followed by O_2 | N_2 and another TEA-enclosed TEMAZ dose as shown in Table 3-3. The flow pattern for 1½ cycles experiment is shown in Figure 3-2. Each step of the exposure sequence was 3 minutes and the flowrate in each line was 10 sccm in total for every step.

Table 3-3. Exposure sequence for 1½ cycle ALD with TEMAZ/O_2 with the low partial pressure of TEA

Cycle	Step	Line A	Line C
1st half cycle Cycle #1	Pre-dose (3 min)	10 sccm He	2 sccm TEA (-10 °C) | N_2 + 8 sccm N_2
	Co-dose (3 min)	10 sccm TEMAZ (40 °C) | He	2 sccm TEA (-10 °C) | N_2 + 8 sccm N_2
	Post-dose (3 min)	10 sccm He	2 sccm TEA (-10 °C) | N_2 + 8 sccm N_2
	Purge (3 min)	10 sccm He	10 sccm N_2
2nd half cycle Cycle #1	Co-reactant (3 min)	10 sccm He	3 sccm O_2 + 7 sccm N_2
	Purge (3 min)	10 sccm He	10 sccm N_2
1st half cycle Cycle #2	Pre-dose (3 min)	10 sccm He	2 sccm TEA (-10 °C) | N_2 + 8 sccm N_2
	Co-dose (3 min)	10 sccm TEMAZ (40 °C) | He	2 sccm TEA (-10 °C) | N_2 + 8 sccm N_2
	Post-dose (3 min)	10 sccm He	2 sccm TEA (-10 °C) | N_2 + 8 sccm N_2
	Purge (3 min)	10 sccm He	10 sccm N_2

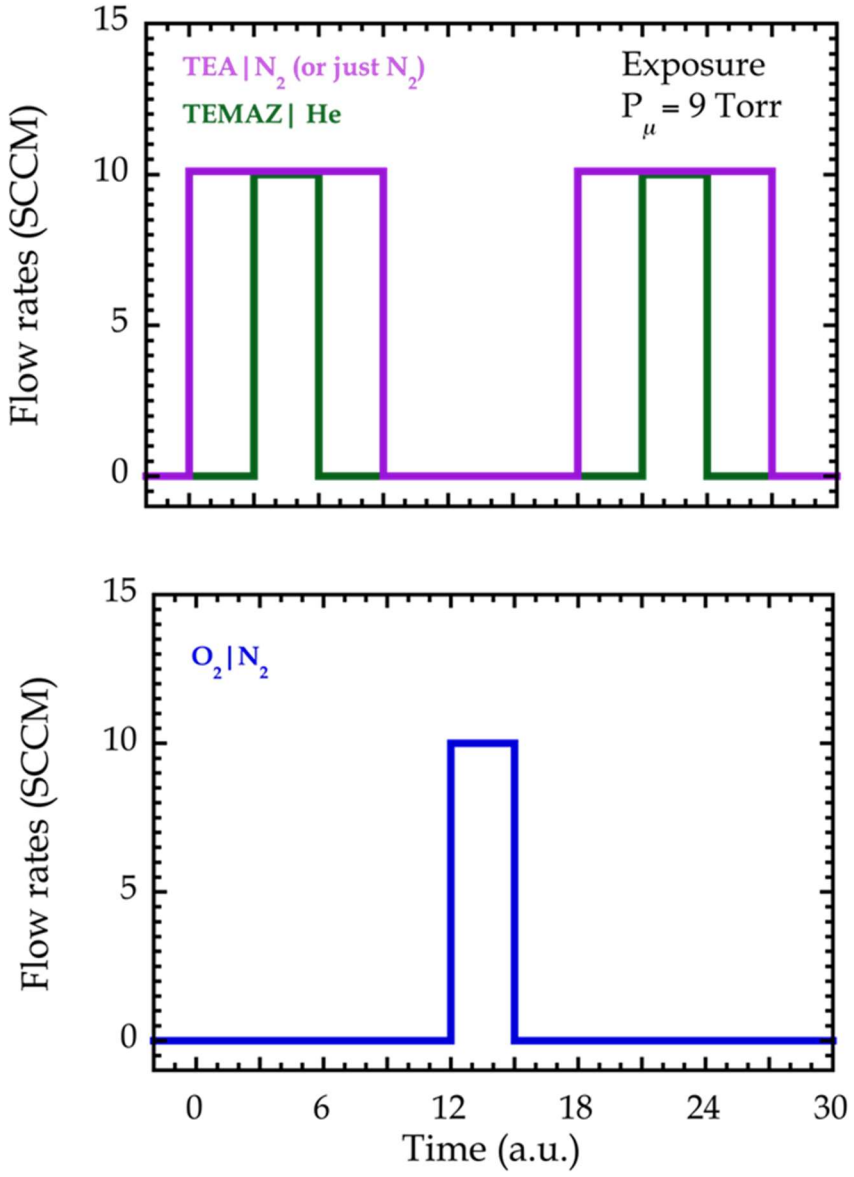

Figure 3-2 Exposure sequence for 1½ cycle experiment with the low partial pressure TEA.

3.1.5 XPS Analysis

Following deposition, composition of the film is studied in the ultrahigh vacuum chamber coupled to the microreactor as described in chapter 2. The pressure of 18 Torr inside the microreactor was brought down to low vacuum by the mechanical pump within ~ 30 minutes and then pumped down to UHV using the ante turbo pump through the bypass valve. The pressure of the main chamber is typically ~10^{-7} Torr right after opening the gate valve to the main chamber. It takes ~ 4 hours to bring down the pressure to ~9.0×10^{-9} Torr. Surface characterization with XPS is then ready. *In vacuo* transfer to the analysis chamber occurs which minimizes possible contamination or oxidation of grown film due to air break. First, line scans of Zr (3d) and O (1s), quick XPS at incremental distances, across y and z axes are conducted. Line scans can be used to determine how thick films are as function of position as seen in Figure 3-3. This is a plot of integrated intensity of Zr(3d) on 4 in. Cu substrate from 1½ cycle experiment without TEA. Line scans were done using aperture 4 with high magnification (1200 μm spot size), zero take-off angle from the substrate to the analyzer, and X-rays generated from the Mg anode. Once the center point of deposition is determined from the line scans, a detailed scan of various elements is performed with repetition and smaller step size to increase the signal to background ratio. A survey scan across the entire binding energy range from 0 to 1000 eV is done and positions of elements of interest are determined. The scanned elements include C (1s), Zr (3d), S(2p), O(1s), N (1s), and Si (2p) or Cu (2p) depending on the substrate. A typical survey scan was done using the same aperture size/magnification as in line scans, take-off angle of 38.5°, and X-rays produced by both Mg and Al anodes.

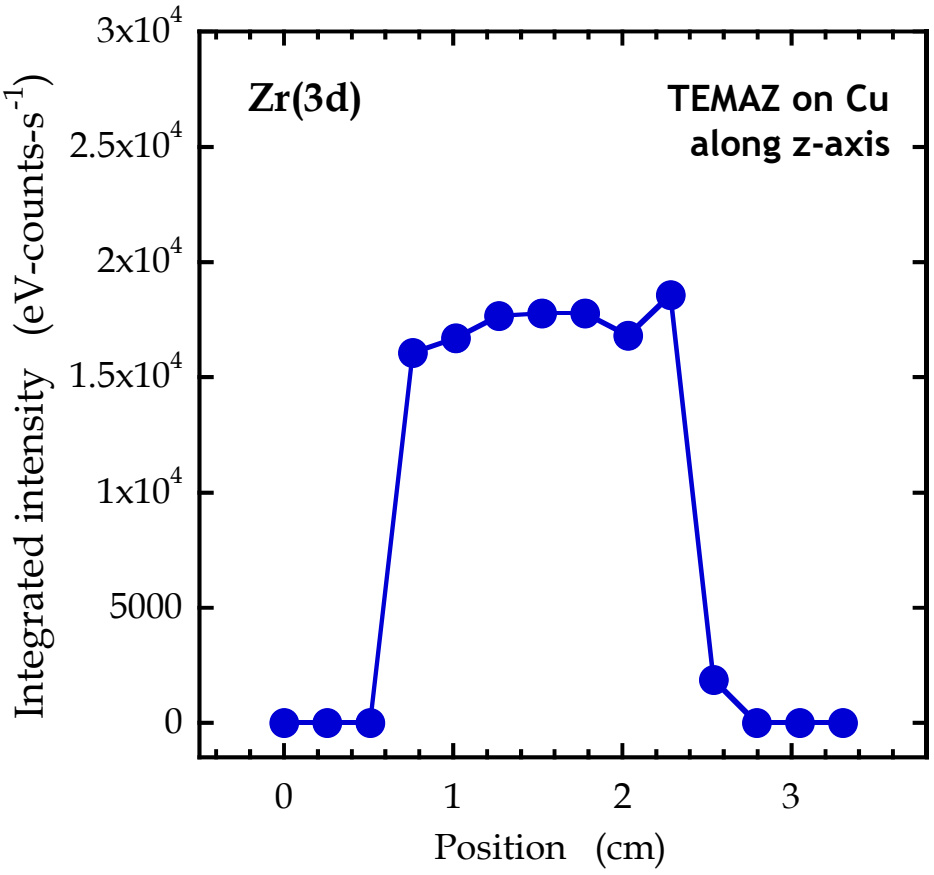

Figure 3-3 A line scan on 4 in. Cu substrate along z-axis for 1½ cycle experiment without TEA (reported in section 3.1.4). Integrated intensity of Zr(3d) as a function of position

3.2 Temperature-Partial Pressure Ratio Study

3.2.1 Sample Preparation

To increase throughput of experiments, a different sample holder was designed. The two-slit sample holder is capable of exposing SiO_2 and Cu substrates to identical experimental conditions simultaneously. Two coupon samples of 1.2 in x 0.4 in are prepared by the same procedure previously described. The sample holder produced different substrate temperatures from the 4 in wafer holder because of their disparity in heat transport properties. According to the temperature calibration curve shown in Figure 2-3, a range of temperatures are selected to study the effect of substrate temperature on selective deposition.

3.2.2 Experiments

Two of many important parameters of selective area ALD, substrate temperature and partial pressure ratio of the metal precursor to co-adsorbate, were studied in a 3 by 3 matrix of the first half-cycle experiments: three substrate temperatures and three concentrations of TEA. Detailed procedure for these experiments are shown in Table 3-4 (a). After 30 minutes of substrate-annealing at 180 °C, the substrate temperature was set to 120, 150, or 180 °C for the actual experiment. The three concentrations correspond to no, low, and high partial pressures of TEA. The high partial pressure of TEA was produced by diluting 2 sccm of TEA | N_2 with 8 sccm of N_2 while the low one was generated by diluting 1 sccm of TEA | N_2 with 9 sccm of N_2. Thus there is factor of two difference between the high and low partial pressures. TEMAZ was in a water bath of 47 °C and TEA in a propylene glycol bath of -10 °C. Delivery lines used for this set of experiments are on three parallel sliding panels as shown in Figure 2-4. One thing to notice is that Table 3-4 has Line B which is not included in the other tables. All three inlets for the

Table 3-4. (a) Exposure sequence for ½ cycle ALD with TEMAZ with high low partial pressure of TEA and (b) vapor pressures of the reactants and their ratios in "low" and "high" cases

(a)

Step	Line A	Line B	Line C
Annealing (30 min)	Substrate annealed at 180 °C No Flow		
Pre-dose (2 min)	10 sccm He	10 sccm N_2	2 sccm TEA (-10 °C) | N_2 + 8 sccm N_2
Co-dose (2 min)	10 sccm TEMAZ (47 °C) | He	10 sccm N_2	2 sccm TEA (-10 °C) | N_2 + 8 sccm N_2
Post-dose (2 min)	10 sccm He	10 sccm N_2	2 sccm TEA (-10 °C) | N_2 + 8 sccm N_2

(b)

Material	Vapor Pressure	Experiment	Partial Pressure Ratio (TEA:TEMAZ)
TEMAZ (47 °C)	0.030 Torr	"Low" TEA	12.1
TEA (-10 °C)	3.6 Torr	"High TEA"	24.2

microreactor were utilized for this set of experiments while only two (A and C) lines were used for experiments described in section 3.1.3-4. Post-deposition characterization of film using XPS was operated in the same procedure as previously described.

3.3 Lewis Acid-Base Complex

Preliminary density functional (DFT) calculations of TMA/H_2O system are done using software called Orca and Q-Chem. Various candidates for the Lewis bases are investigated to study how a Lewis base changes properties of an adduct formed with TMA. Molecules with N, O, or P central groups are studied as well as effects of van der Waals interactions and steric hindrance between ligands during adduct formation. Electron withdrawing groups such as CF_3, C_2F_5 ligands are compared to electron donating groups, CH_3 and C_2H_5 ligands. The effect of introducing bare TMA vs. a Lewis acid-base complex, TMA-NH_3, to a surrogate for OH-terminated SiO_2 surface, H_3SiOH, is studied as well. The simulation results will suggest whether exposing TMA-NH_3 adduct is beneficial or not in terms of achieving selective growth. The DiStasio Research Group, our collaborators from Cornell University, provided the simulation data reported in this thesis.

4. Results and Discussions

4.1 Co-adsorption of TEMAZ and EDT/TEA

4.1.1 Effect of EDT

Sulfur is a well-known poison in the petroleum industry, reducing activity of transition metal catalysts during coal gasification [25]. As a sulfur-containing molecule, EDT is particularly used for its poisoning effect on metals. Employing intrinsic affinity of sulfur and its

difference towards dielectric (SiO_2) and metal (Cu) surfaces, selective deposition of Zr was obtained for a set of conditions. Figure 4-1 compares intensities of Zr(3d) peaks from XPS on SiO_2 and Cu, shown on left and right, respectively [26]. The black spectra are data obtained from five-minute dose of TEMAZ without EDT. The blue lines represent results of a co-adsorption experiment with 2 sccm of EDT (-10°C) | N_2, or "low" concentration of EDT. Lastly, the red spectra are from use of 10 sccm of EDT (0°C) | N_2, denoted "high" concentration of EDT in the figure. The same color scheme of black, blue, and red to illustrate results from no, low, high concentration of a co-adsorbate, respectively, is used for figures presented here on. Zr deposition is seen on both substrates in absence of EDT. For the low concentration of EDT co-exposure, deposition of Zr on SiO_2 was not perturbed while that on Cu was entirely suppressed. A possible explanation for this selective growth is that sulfur acts as a site-blocking layer on Cu whereas it does not bind as strongly on SiO_2. The absence of S peaks on SiO_2 substrate also confirmed that the co-adsorbate species has stronger affinity toward the metal surface. The calculated partial pressure ratio of EDT to TEMAZ from bath temperatures and flowrates of corresponding streams is 5.9:1. For the high concentration, growth inhibition is observed on both substrates. A small, broad peak on SiO_2 is a plasmon peak from the substrate which appears near the binding energy of Zr(3d). The ratio of partial pressures of EDT to TEMAZ was 66:1. When exposure of EDT was increased by a factor of ~10, selectivity was lost, indicating that the partial pressure ratio of a metal precursor to a co-adsorbate is a significant factor in achieving selective growth.

Sulfur, the functional group of EDT, was only observed on Cu. The intensities of S(2p) peaks for high and low concentration EDT cases are shown in Figure 4-2. The high concentration EDT resulted in the most sulfur on the surface and ~81% of that was observed from the intermediate partial pressure of EDT. These intensities can be converted into atomic density of

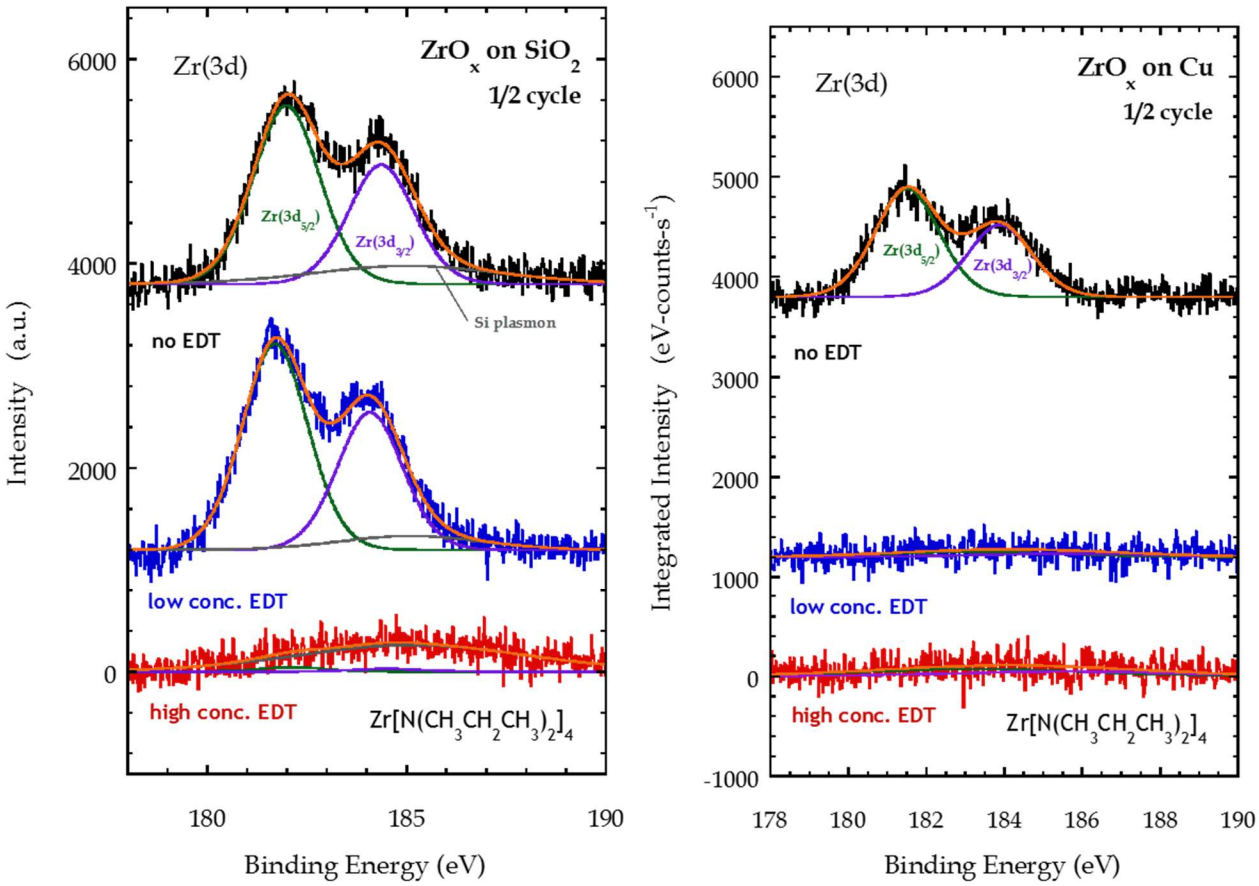

Courtesy: Wenyu Zhang

Figure 4-1 XP spectra of Zr(3d) for experiments with no, low, and high partial pressures of EDT on SiO_2 (left) and Cu (right) substrates

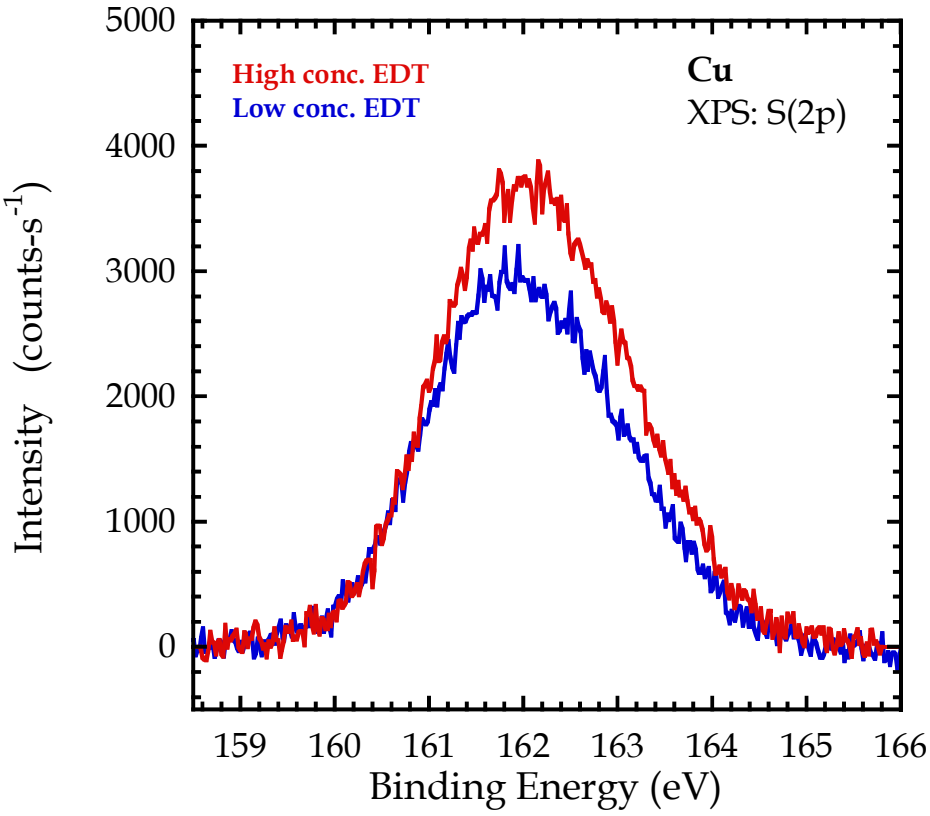

Figure 4-2 XP spectra of S(2p) on Cu for the high and low EDT experiments

sulfur, 3.07 and 2.48 × 10^{15} S atoms·cm^{-2}, for high and low partial pressures of EDT, respectively. Approximately a factor of 4.1 and 3.3 for the high and low exists when compared to a monolayer coverage of S, or 7.5 × 10^{14} S atoms·cm^{-2} in atomic density, equivalent to 0.43 monolayer coverage of sulfur on Cu (111) surface. This number represents the maximum surface coverage of sulfur on that specific surface [27]–[29]. Considering EDT has two sulfur atoms in one molecule, one can determine that ~2.0 and 1.7 monolayers of EDT are present on Cu surfaces from experiments with the high and low partial pressures of EDT. However, the mechanism by which EDT suppressed growth completely on SiO_2 at high EDT remains unclear since no S was observed on that substrate. EDT demonstrated a strong history effect; lingering thiol species contaminated experiments without any co-adsorbate molecules. Thus, the study of selective area ALD with thiol was not further pursued and it was replaced by TEA after system cleaning.

The cleaning procedure to remove lingering thiol involves an acid and several organic solvents. An hour of sonication in 50% nitric acid is conducted first, to dissolve as much thiol as possible from stainless steel walls. Then the cleaned components are flushed with lots of DI water to expel the dissolved sulfur from them. This step is often useful for long flexible hoses because sulfur tends to linger in them without flushing. Human nose is used to detect the existence of sulfur (sulfur can be detected in ppm level) after the acid bath and longer sonication in the acid is carried out if necessary. Afterwards, 30-mintue sonication in three baths of organic solvents are used: trichloroethylene, acetone, and isopropyl alcohol. Trichloroethylene removes any hydrocarbons, while isopropyl alcohol (IPA) eliminates chlorine originated from trichloroethylene. In addition, acetone and IPA eliminate any water from the parts being cleaned.

After four steps of sonication, the cleaned parts are covered with foil and left in air overnight to let the remaining organic solvents evaporate before put back on delivery lines.

4.1.2 Effect of TEA

Relative Zr(3d) intensities from the experiments with high, low, and no partial pressure of TEA are shown in Figure 4-3. For the case with no TEA, the same amount of Zr was deposited on both SiO_2 and Cu as represented in the figure. For the intermediate partial pressure of TEA, growth is suppressed by ~49% on SiO_2 while growth is completely blocked on Cu. Selective deposition was achieved under this set of conditions in which the partial pressure ratio of TEA to TEMAZ was 47.8:1. When this ratio was increased by a factor of five to 240:1 by not diluting the TEA | N_2 stream for the high concentration of TEA, no deposition of Zr was observed on both substrates. A similar trend of the amount of Zr deposited with respect to concentration of the co-adsorbate was observed as in the EDT study; however, the mechanism behind selectivity may be different. In contrast to a site-blocking layer of EDT, TEA possibly participated in reversible adsorption of TEMAZ. Having an analogous chemical structure to a ligand of TEMAZ, TEA molecules were present before, during, and after TEMAZ exposure to minimize the extent of decomposition of TEMAZ. Pristine TEMAZ may have left the Cu surface after exposure.

Nitrogen intensities on Cu substrate for the three experiments are compared in Figure 4-4. There is no significant change in intensity of N(1s) as a function of TEA concentration, which also may support the idea of TEA not acting as a site-blocking layer. Not only from TEA, the nitrogen signal could come from ligands of TEMAZ as well, but N intensity is too small, if not zero, to draw a definitive conclusion.

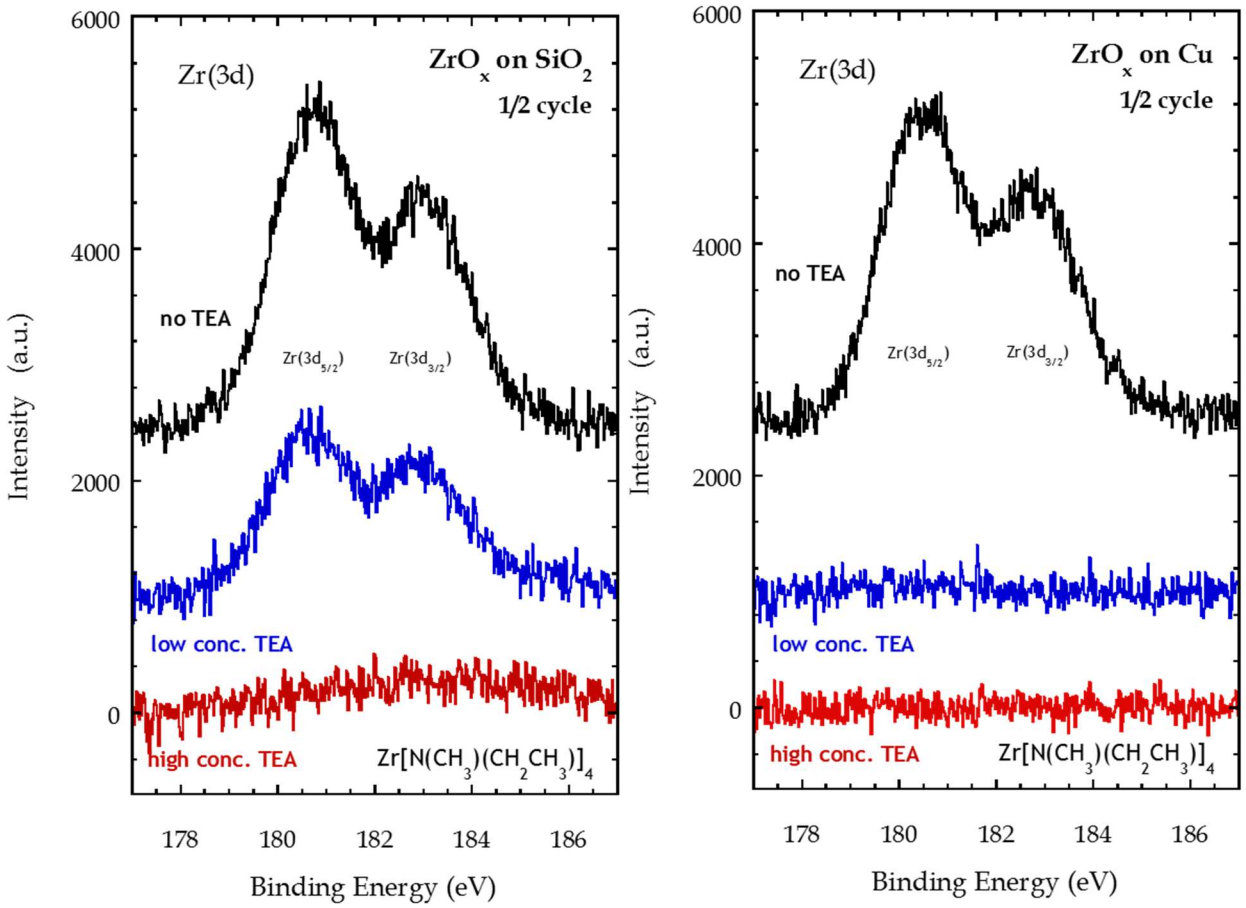

Courtesy: Wenyu Zhang

Figure 4-3 XP spectra of Zr(3d) for experiments with no, low, and high partial pressures of TEA on SiO_2 (left) and Cu (right) substrates

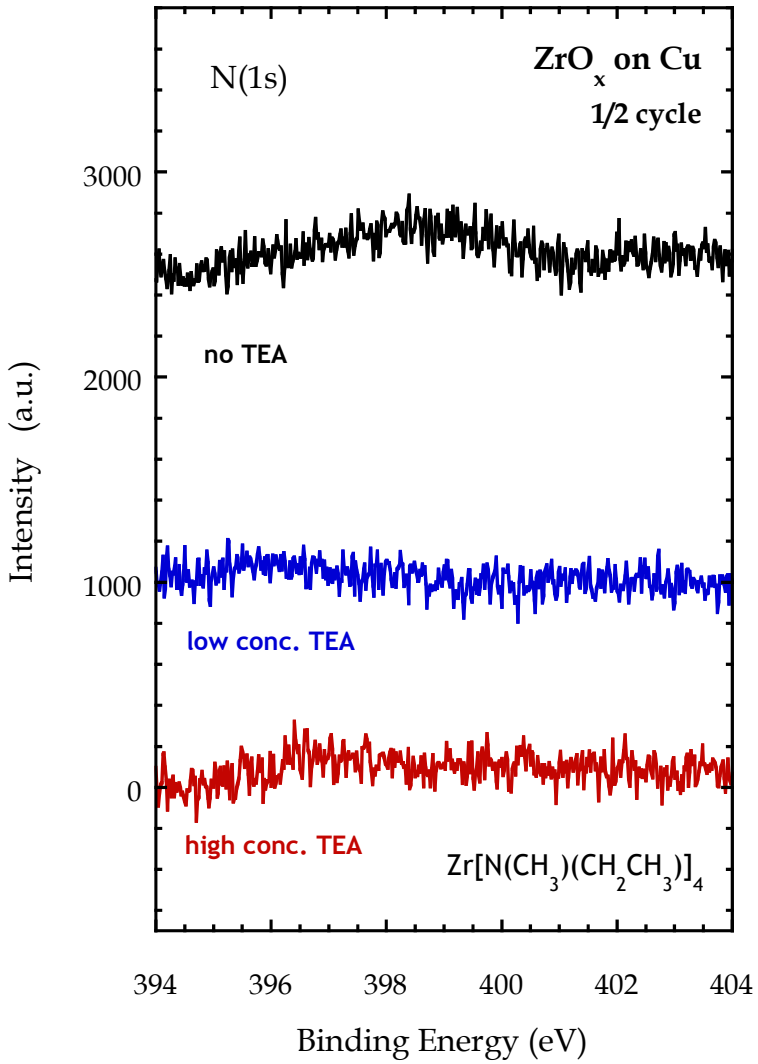

Figure 4-4 XP spectra of N(1s) on Cu for the no, low, and high TEA experiments

4.1.3 1½ Cycle Study

The same conditions for the half-cycle experiment with the intermediate partial pressure of TEA in which selective growth was achieved were employed in a 1½ cycle study. 1½ cycle experiments with and without TEA were conducted to investigate the effect of co-reactant and co-adsorbate in depositing thin films on selective areas using ALD. Zr(3d) intensities from these experiments on SiO_2 and Cu are plotted in Figure 4-5. The similar area underneath the peaks, represented in black, indicate that without TEA, film grew approximately the same amount on both substrates. This is consistent with the half-cycle experiment without TEA described earlier. From the 1½ cycle without TEA, the Zr atomic density on SiO_2 was 1.1×10^{15} Zr atoms·cm^{-2}, 1.8 times greater than that from the bare half-cycle result, 6.22×10^{14} Zr atoms·cm^{-2}. This number may be slightly smaller than two due to possible attenuation of Zr (3d) signal for thicker films. 6.19×10^{14} Zr atoms·cm^{-2} is deposited on SiO_2 from 1½ cycle experiment with the use of TEA, ~ 56% compared to the without-TEA case. This ratio of Zr atomic densities with TEA to without TEA in 1½ cycle experiment is very similar to that observed in a half-cycle study, 3.06×10^{14} Zr atoms·cm^{-2} with TEA vs. 6.22×10^{14} Zr atoms·cm^{-2} without TEA. This consistency in atomic densities suggests that TEA has the same effect on achieving selective deposition in both first- and multiple-cycle experiments. On Cu surface, growth of Zr is completely blocked in presence of TEA, as discovered previously. Zr intensities observed on both substrates using the intermediate partial pressure of TEA in the half and 1½ cycles are summarized in Figure 4-6. A linear relation for all four lines shown in the figure is expected since the amount of film growth is a function of the number of cycles in ALD processes, given sufficient exposure time. A factor of ~2 increase from a half cycle to 1½ cycle corresponds well to the number of TEMAZ dose in each experiment.

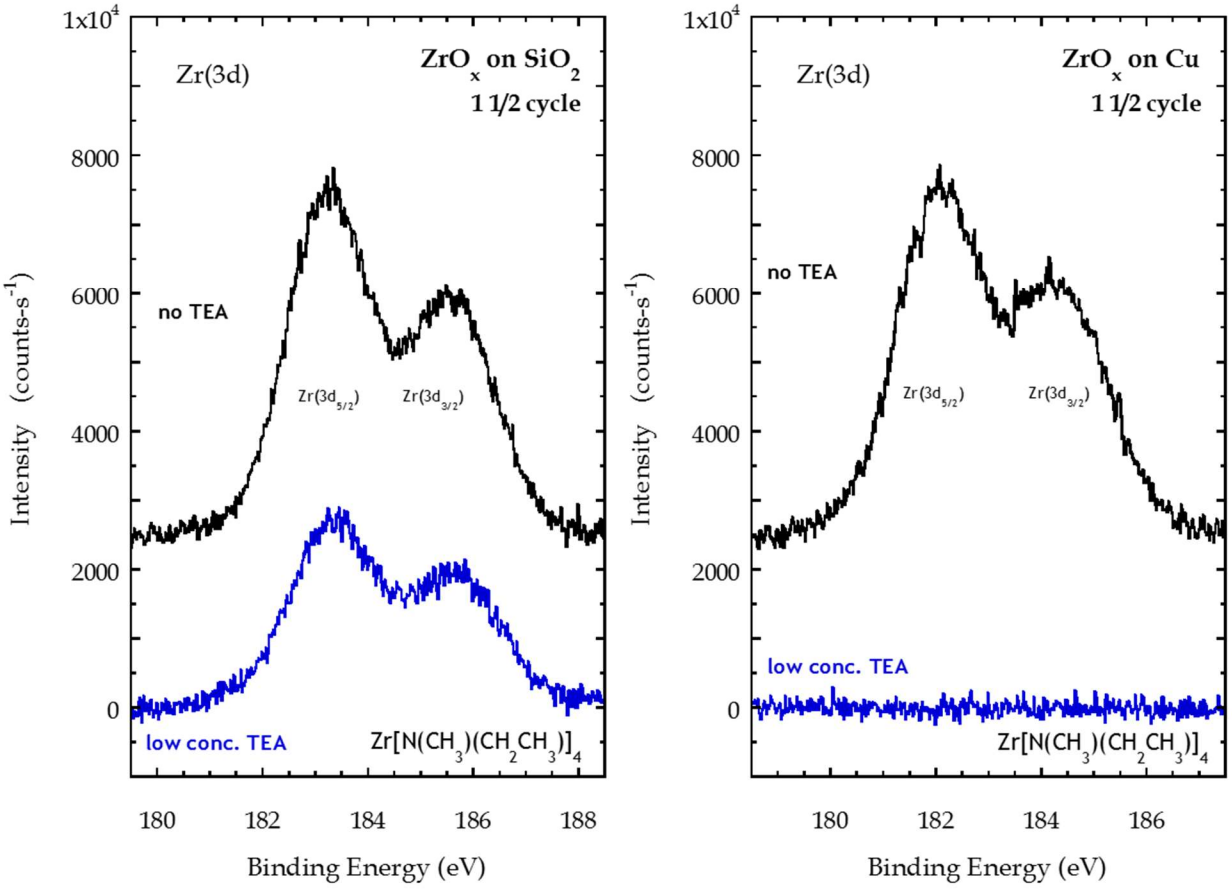

Figure 4-5 XP spectra of Zr(3d) for 1½ experiments with no and low partial pressures of TEA on SiO_2 (left) and Cu (right) substrates

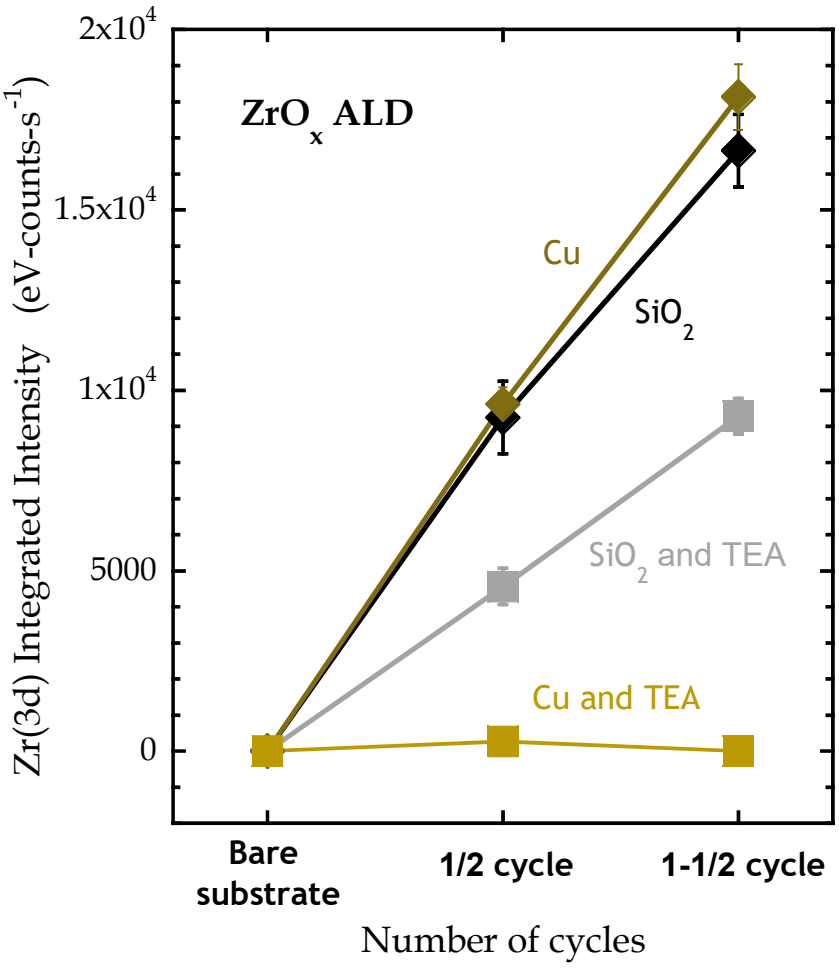

Figure 4-6 Integrated intensities of Zr(3d) for ½ and 1½ cycle experiments with/without TEA on both SiO_2 and Cu substrates

4.2 Effect of Substrate Temperature and Partial Pressure Ratio

4.2.1 Simulation Model (Matlab)

Kinetic simulations for calculations of the surface coverage are also conducted to study effects of exposure time and partial pressure ratio on deposition of a metal precursor. The two governing equations are based on a first order ODE for both the co-adsorbate and metal precursor. The two equations are given as the following,

$$\frac{d\theta_A}{dt} = \frac{S_A F_A}{n_s}(1 - \theta_A - \theta_B) - k_{d,A}\theta_A$$

$$\frac{d\theta_B}{dt} = \frac{S_B F_B}{n_s}(1 - \theta_A - \theta_B)^2 - k_{d,B}\theta_B^2$$

in which θ is surface coverage, S for probability of adsorption, F for flux, n_s for surface density of active sites, and k_d for desorption coefficient. The coefficient for desorption was modeled to follow Arrhenius equation and the activation energies for desorption of the two reactants are chosen such that that of the metal precursor is greater in magnitude than the other in this simulation. These two equations signify that the rate of change in surface coverage of a species is dependent on the number of unoccupied active sites (possible adsorption) and surface coverage itself (possible desorption). A first order kinetics were selected for adsorption and desorption for the co-adsorbate species, while a second order reactions were chosen for the metal precursor. These assumed orders for the gas-surface reaction are consistent with the mechanism by which each reactant binds to a surface. The co-adsorbate would bind to a surface via molecular chemisorption while the metal precursor would bind through dissociative chemisorption.

The initial coverage of A in the co-exposure step is taken as the steady-state value in the absence of B, equivalent to the pre-dose step. These values are calculated with

parameters/equations in Table 4-1. The final θ_B at the end of co-exposure is plotted against exposure time at a partial pressure ratio of 12.1:1, co-adsorbate to metal precursor, in Figure 4-7. In absence of co-adsorbate, labeled as "No Co-adsorbate" case in the figure, the surface coverage of the metal precursor reaches 99% of the steady state value after 0.26 seconds, marked by the red vertical line. In the "12.1:1" case, the same partial pressure ratio of co-adsorbate to metal precursor in the low TEA experiment (section 4.2.2) was used. The co-adsorbate species not only lowered the surface coverage of the metal precursor, but also substantially extended the exposure time required to reach the steady state value for coverage. With the partial pressure ratio of 12.1, co-adsorbate to precursor, the steady state surface coverage of metal precursor was 0.0063, solved analytically. When the blue points were fit to an equation that has one minus an exponentially decaying term (the green curve in Figure 4-7), the time constant, or time to reach steady state, was calculated to be 1240 seconds. The delay in reaching a full coverage is due to presence of co-adsorbate which competes with the metal precursor for surface active sites, delaying its nucleation. More surface blocking by co-adsorbate, more difficult for precursors to adsorb on the surface during co-exposure. If the metal precursor is exposed for 0.26 seconds, a saturated coverage would be formed on a surface that co-adsorbate does not chemisorb. In contrast, given the same exposure time, the surface coverage on the other surface on which the co-adsorbate species interact is still on the order of 10^{-6}, thus depositing on one surface but not on the other.

One must keep in mind that this simple model is not fully representative of what occurs in reality. In this simple model, the co-adsorbate and metal precursor compete for surface active sites and do not interact with each other, whereas for TEMAZ and TEA, they may go through

Table 4-1. Parameters/equations used in the simple model to generate the two curves in Figure 4-7.

Parameters	Values/Equations
Substrate temperature, T	150 (°C)
Pressure of reactants, P_A, P_B	1.21, 0.1 (Torr)
Probability of adsorption, S_A, S_B	1, 0.002
Density of active sites, n_s	10^{19} (sites·m^{-2})
Energy barrier of desorption, $E_{d,A}$/ $E_{d,B}$	20/25 (kcal/mol)
Flux of reactants, F_A	$\frac{N_A \cdot P_A}{(2\pi MW_A RT)^{1/2}}$
Coefficient for desorption, $k_{d,A}$	$A \cdot \exp\left(-\frac{E_{d,A}}{RT}\right)$

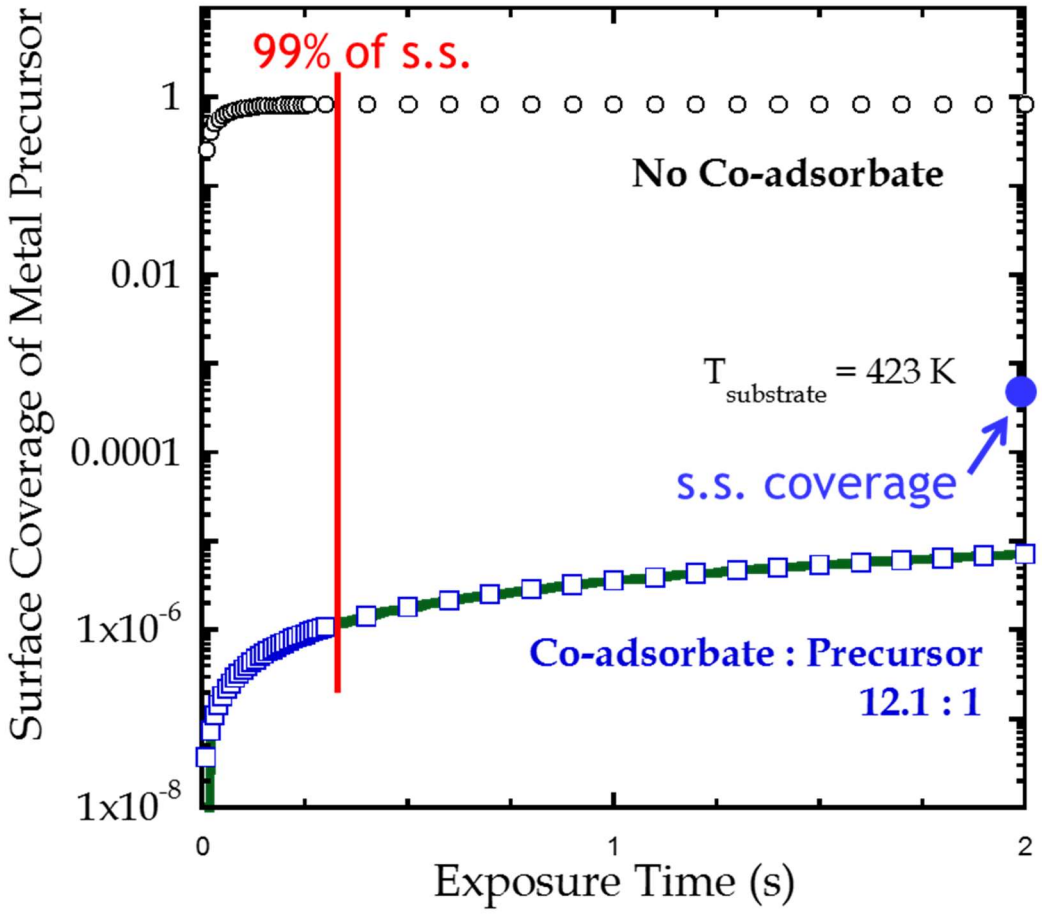

Figure 4-7 Surface coverage as a function of exposure time from the simulation model. The red vertical line is when the surface coverage reaches its steady state for the no co-adsorbate case.

ligand exchange reactions. Even though this model needs further improvement, it can indicate the effect of the co-adsorbate and how it delays nucleation of the film.

4.2.2 Effect of Temperature

Annealing at 180 °C for 30 minutes removed a satellite peak around binding energy of 942 eV near Cu 2p XPS spectra. Detection of the satellite peak corresponds to presence of CuO which indicates a high degree of oxidation state of metallic Cu [30]. Therefore, all the nine experiments at no, low, high partial pressure of TEA at 120, 150, 180 °C were carried out after 30 minutes of annealing at 180 °C. Atomic density of Zr from experiments of 3 by 3 matrix are on SiO_2 and Cu are plotted in Figure 4-8 and 4-9, respectively. The partial pressure ratio of 0, 12.1, and 24.2 are equivalent to effective ratio of TEA to TEMAZ in the reaction zone for no, low, and high TEA concentrations as shown in Table 3-4 (b). For SiO_2, the highest suppression of Zr growth is observed at the high TEA cases in general. As seen in Figure 4-8, the substrate temperature seems to have different effects. For the low partial pressure of TEA, temperature of 180 °C produced the least amount of film while at the high pressure of TEA, least Zr was observed at 150 °C. For Cu (Figure 4-9), Zr growth is completely inhibited at all three temperatures at high partial pressure of TEA. The intermediate pressure of TEA gave a minimum at 180 °C and a maximum at 150 °C.

4.2.3 Effect of Partial Pressure Ratio

As in the simulation, a general trend of atomic density as a function of partial pressure ratio can be seen on both SiO_2 and Cu substrates: more dose of TEA, less deposited Zr. TEA in the reaction zone may participate in preventing TEMAZ from dissociation to form a covalent

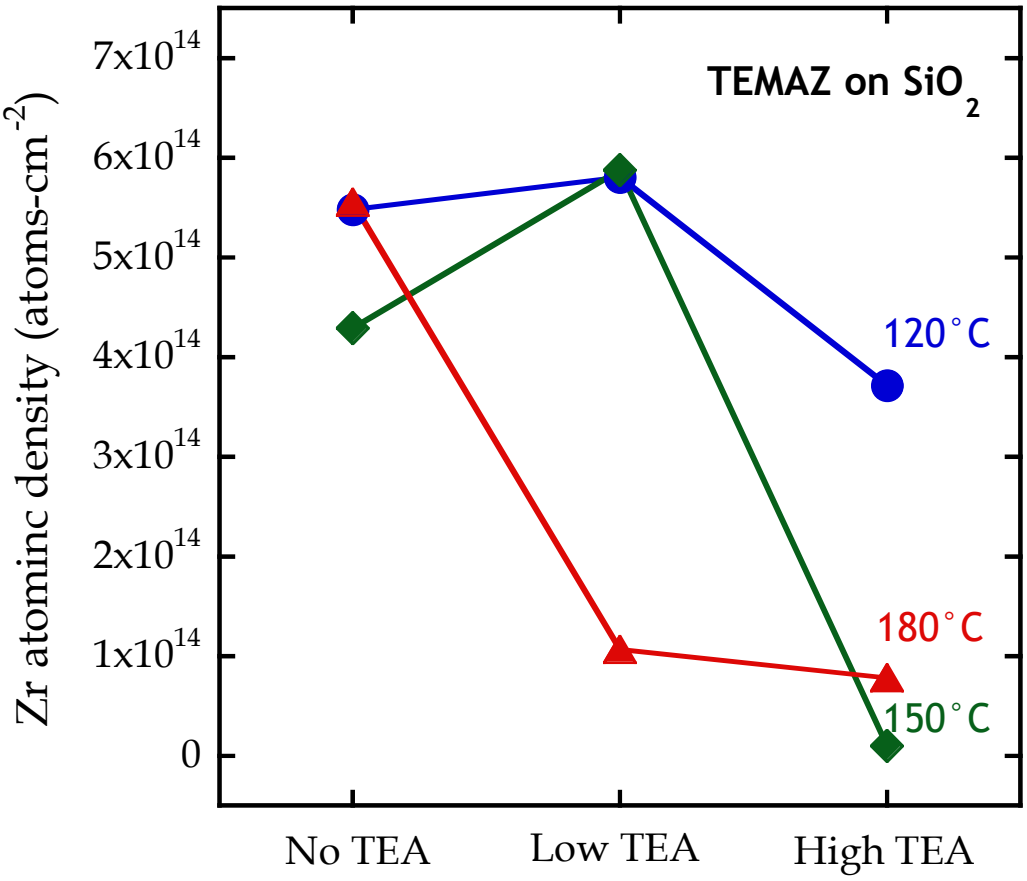

Figure 4-8 Atomic density of Zr on SiO_2 for no, low, and high TEA experiments at various temperatures.

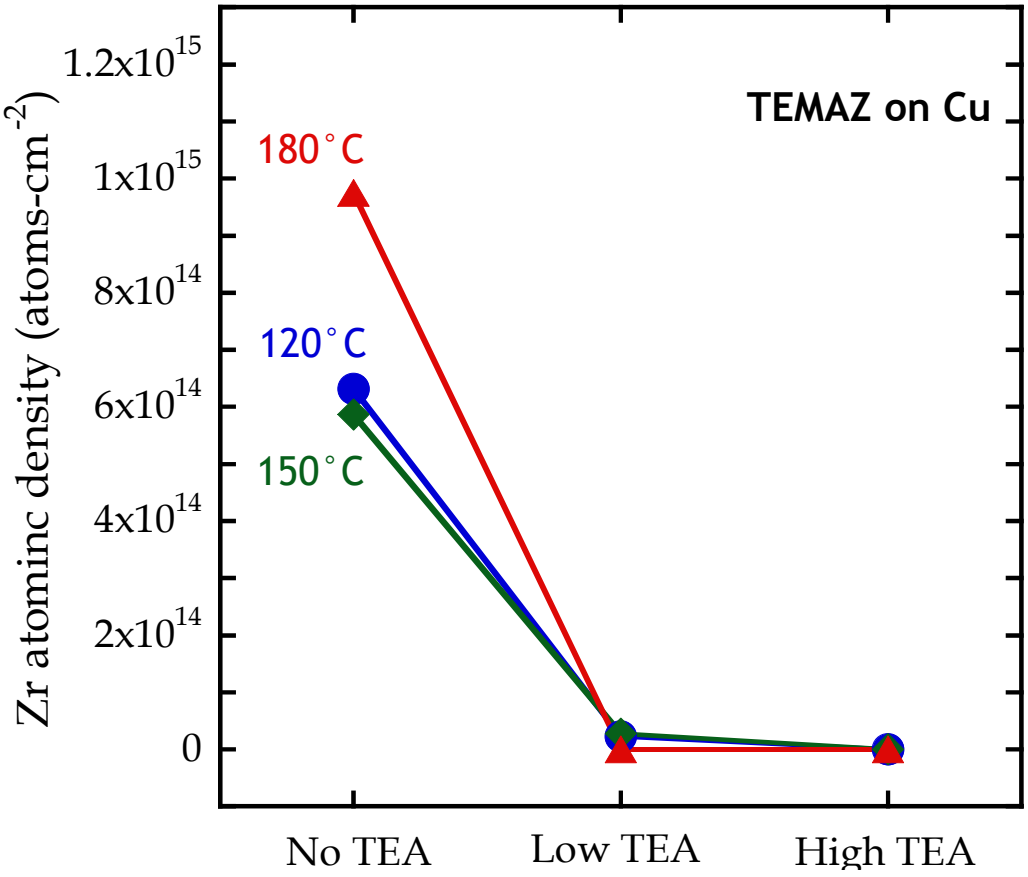

Figure 4-9 Atomic density of Zr on Cu for no, low, and high TEA experiments at various temperatures.

bond upon contact with the substrate as discussed in chapter 4.1.2. By comparing Figure 4-8 and 4-9, selective chemisorption is accomplished to some extent at for all three substrate temperatures with low or high partial pressure of TEA. Even though growth of Zr on Cu is completely blocked, growth on SiO_2 is suppressed to ~9.2×10^{13} Zr atoms·cm^{-2} for 180 °C in presence of TEA. At the substrate temperature of 150 °C, high partial pressure of TEA inhibited deposition of Zr on both substrates while the intermediate pressure of TEA resulted in 2.8×10^{13} Zr atoms·cm^{-2} on Cu without disturbing growth on SiO_2. Since the amount of growth on Cu is within error level, one could say selective deposition is achieved for this set of conditions. However, since there likely is Zr on Cu surface which would act as nucleation sites, this set of conditions may not be suitable for a multiple cycle study. At 120 °C, low pressure of TEA resulted in 2.3×10^{13} Zr atoms·cm^{-2} on Cu while high pressure of TEA completely blocked on Cu and suppressed down to 3.7×10^{14} Zr atoms·cm^{-2} on SiO_2. It can be concluded that a partial pressure ratio of TEA to TEMAZ between 12.1 and 24.2 is a threshold of TEA to start disrupting growth on SiO_2 at this temperature. In contrast, TEA has shown stronger effect on Cu surface since presence of TEA at all substrate temperatures showed almost zero, if at all, deposition of the metal precursor.

4.3 Effect of Adduct Formation

First, adduct formation of TMA with two different Lewis bases, NH_3 and H_2O, are performed to determine with which of the two molecules TMA prefers to bind to and react for methane elimination. Change in potential energy during a methane elimination process for the two complexes, TMA-NH_3 and TMA-OH_2, is plotted in Figure 4-10. Geometry optimization of molecules/complexes and determination of transition states are conducted with B3LYP/6-31G*

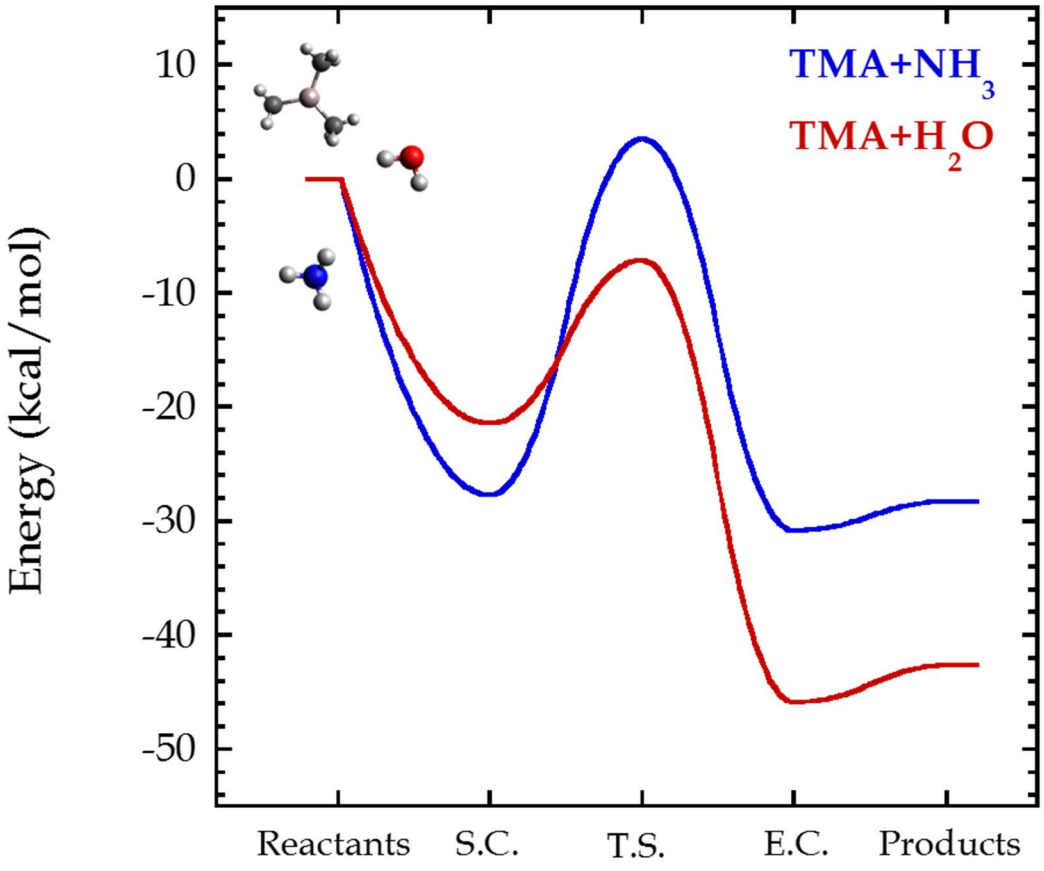

Figure 4-10 DFT calculations of energy change during adduct formation of TMA with NH_3 and H_2O and methane elimination reactions. Energies are calculated at infinitely separated reactants, starting complex (S.C.) of methane elimination, transition state (T.S.), ending complex (E.C.), and products

with D3 (dispersion correction) level of theory. All energies obtained by this method are referenced to zero, or energy at infinite separation of reactants. For reaction of TMA with NH_3, shown in red, the reactants are stabilized by -27.7 kcal/mol when a Lewis acid-base complex without any activation energy barrier. TMA-NH_3 adduct is more stable compared to TMA-OH_2, a stabilization energy of -21.4 kcal/mol for the latter. Does this mean TMA prefers to react with ammonia than water? The binding energy of an adduct does not provide complete interpretation of reaction mechanisms with different Lewis bases. Elimination of CH_3 from TMA and H from the Lewis base needs to be considered to investigate how the binding is different once a covalent bond is formed between Al and N/O. Adduct as the starting complex, energy change along transition state and ending complex post-methane elimination is shown. The energy barrier of TMA taking H from H_2O is 14.3 kcal/mol compared to 31.2 kcal/mol for NH_3 with respect to the vacuum level, indicating that reaction of TMA with H_2O is more kinetically favorable than the other. Thermodynamically favorable pathway can be determined by comparing potential energies after methane elimination (ending complex), 30.8 kcal/mol for NH_3 and 45.9 kcal/mol for H_2O. From preliminary calculations of relative energy throughout a methane elimination process, TMA-OH_2 adduct has weaker binding but it is both kinetically and thermodynamically favorable than the TMA-NH_3. Further study needs to be done, but one can draw a conclusion that H_2O introduced in a second half-cycle of ALD may replace lingering NH_3 and prevent N atom from incorporating into the film.

To study the effect of co-exposure of NH_3 on deposition of TMA, bare TMA and TMA-NH_3 complex are introduced to a simple model of hydroxylated Si surface, SiH_3OH. As seen in Figure 4-11, pristine TMA reacts with the OH group on the surface similarly to OH from water, the latter represented in the black dashed line; TMA is stabilized by -19.0 kcal/mol through

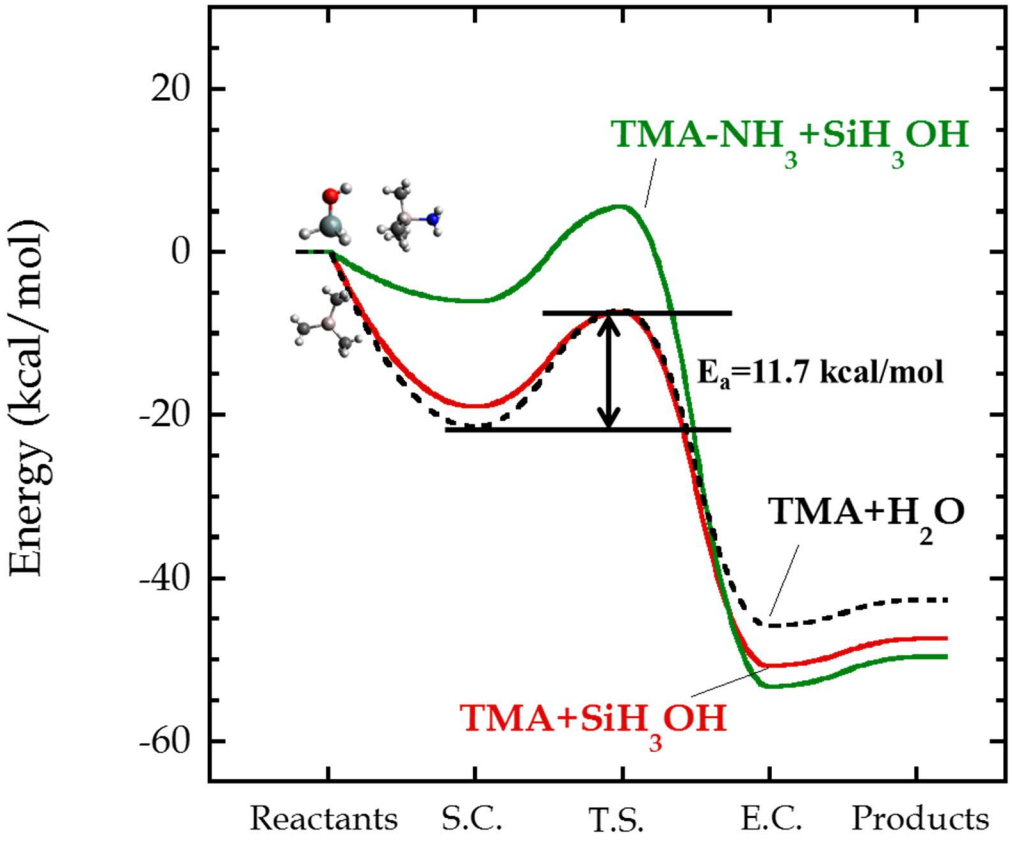

Figure 4-11 DFT calculations of energy change during methane elimination reaction between TMA/SiH_3OH and TMA-NH_3/SiH_3OH. TMA/H2O shown in dashed line for reference Energies are calculated at infinitely separated reactants, starting complex (S.C.) of methane elimination, transition state (T.S.), ending complex (E.C.), and products

chemisorption of Al on O, goes through a barrier of 11.7 kcal/mol for methane elimination, and forms a covalent bond between Al and O from the surface post-elimination, with stabilization energy of 47.5 kcal/mol. Comparable energy changes to those from the reaction with H_2O can be explained by similar chemical structures between H_2O and SiH_3OH. The surface species can be formed by replacing a H from H_2O with SiH_3.The difference in electronegativity of H and SiH_3 may not be significant enough (2.2 for H and 1.9 for Si) to affect the binding of O with another species. When preformed TMA-NH_3 adduct is introduced to the same surface species, they bind with comparatively small energy, 6.1 kcal/mol. This weakened chemisorption of TMA-NH3 to the OH group can be explained by how the empty p orbital of Al is already partially occupied by a pair of electrons from N and is not as active as pristine TMA. The activation energy for methane elimination is 11.7 kcal/mol but it is much higher than the dissociation energy, or the energy needed to return to the reactants, (6.1 kcal/mol). However, higher barrier does not imply that the reaction does not occur; having excess reactants will drive the reaction towards the product and it is also thermodynamically favorable due to a high stabilization energy of 49.72 kcal/mol. Weak bonding between the complex and surface species may allow selective deposition on SiO_2 and Cu, the purpose of this project. Reactivity of TMA may be weakened enough by formation of an adduct with NH3 to not grow on Cu but weakened just enough that TMA still deposits on SiO_2. Further study with Cu surface needs to be done to confirm plausibility of selective deposition. In addition, the degree of weakening will be manipulated by changing the Lewis base by putting longer chains on N atom or putting a ring structure like pyridine.

5. Conclusions

We have examined different methods/mechanisms to achieve selective-area growth by introducing the co-adsorbate species in an ALD process. The two co-adsorbate species used were EDT and TEA. First, the presence of EDT under an appropriate partial pressure completely inhibited growth on Cu without any disruption on SiO_2. However, a greater partial pressure of EDT blocked deposition of TEMAZ on both substrates. We proposed that EDT might have formed a blocking layer on Cu and prohibited growth, based on ~two-monolayer coverage of EDT detected by XPS. The second co-adsorbate species, TEA, resulted in similar behavior; under intermediate partial pressure, selectivity was achieved, while a higher pressure completely blocked growth on both substrates. In contrast to EDT, TEA did not remain on the substrates, which might indicate reversible adsorption by TEA. The identical experimental conditions with TEA capable of selective growth were extended to 1½ cycle experiment. TEA suppressed growth on SiO_2 in the higher cycle, as observed in ½ cycle, but that on Cu was still completely inhibited.

Substrate temperature and partial pressure ratio of TEA to TEMAZ were also investigated. The ratios of 12.1:1 and 24.2:1 (TEA:TEMAZ) blocked most growth, if not all, on Cu. There are varying temperature effects on SiO_2, but generally, less growth is observed at higher temperatures. For the 12.1:1 case, the substrate temperature of 180 °C resulted in least growth while TEA in 24.2:1 ratio produced least growth for 150 °C.

Preliminary DFT calculations on the most-studied ALD chemistry, TMA/H_2O, were conducted in collaboration with the Distasio research group. By reducing the high reactivity of TMA via adduct formation, TMA may still be reactive enough to deposit on one surface but weakened enough to bind on the other. When preformed TMA-NH3 adduct is introduced to

SiH_3OH, a surrogate for OH-terminated SiO_2, the binding of Al-O is weakened by 13 kcal/mol, compared to binding between bare TMA and SiH_3OH. However, the activation energy for methane elimination reaction remains unchanged. Thus, we have weakened the initial binding of TMA to a surface by formation of the adduct without modifying the process kinetically.

References

[1] G. E. Moore and L. Fellow, "Cramming More Components onto Integrated Circuits," vol. 86, no. 1, pp. 82–85, 1998.

[2] R. W. Johnson, A. Hultqvist, and S. F. Bent, "A brief review of atomic layer deposition: from fundamentals to applications," *Mater. Today*, vol. 17, no. 5, pp. 236–246, 2014.

[3] M. Leskelä and M. Ritala, "Atomic layer deposition (ALD): From precursors to thin film structures," *Thin Solid Films*, vol. 409, no. 1, pp. 138–146, 2002.

[4] S. M. George, "Atomic layer deposition: An overview," *Chem. Rev.*, vol. 110, pp. 111–131, 2010.

[5] M. Leskelä and M. Ritala, "Atomic Layer Deposition Chemistry: Recent Developments and Future Challenges," *Angew. Chemie Int. Ed.*, vol. 42, no. 45, pp. 5548–5554, 2003.

[6] F. Sadat, M. Hashemi, C. Prasittichai, and S. F. Bent, "A New Resist for Area Selective Atomic and Molecular Layer Deposition on Metal − Dielectric Patterns," *J. Phys. Chem. C*, vol. 118, no. 20, pp. 10957–10962, 2014.

[7] A. Ulman, "Formation and Structure of Self-Assembled Monolayers," *Chem. Rev.*, vol. 96, no. 4, pp. 1533–1554, 1996.

[8] A. Kumar and G. M. Whitesides, "Features of gold having micrometer to centimeter dimensions can be formed through a combination of stamping with an elastomeric stamp and an alkanethiol 'ink' followed by chemical etching," *Appl. Phys. Lett.*, vol. 63, no. 14, pp. 2002–2004, 1993.

[9] A. Kumar, H. a. Biebuyck, and G. M. Whitesides, "Patterning Self -Assembled Monolayers: Applications in Materials Science," *Langmuir*, vol. 10, no. 8, pp. 1498–1511, 1994.

[10] Y. Xia, M. Mrksich, E. Kim, and G. M. Whitesides, "Microcontact Printing of Octadecylsiloxane on the Surface of Silicon Dioxide and Its Application in Microfabrication," *J. Am. Chem. Soc.*, vol. 117, no. 37, pp. 9576–9577, 1995.

[11] M. Yan, Y. Koide, J. R. Babcock, P. R. Markworth, J. A. Belot, T. J. Marks, R. P. H.

Chang, M. Yan, Y. Koide, J. R. Babcock, P. R. Markworth, J. A. Belot, and T. J. Marks, "Selective-area atomic layer epitaxy growth of ZnO features on soft lithography-patterned substrates Selective-area atomic layer epitaxy growth of ZnO features on soft lithography-patterned substrates," pp. 1–4, 2001.

[12] H. Lim, C. Carraro, R. Maboudian, M. W. Pruessner, and R. Ghodssi, "Chemical and thermal stability of alkanethiol and sulfur passivated InP(100)," *Langmuir*, vol. 20, no. 3, pp. 743–747, 2004.

[13] C. L. McGuiness, A. Shaporenko, C. K. Mars, S. Uppili, M. Zharnikov, and D. L. Allara, "Molecular self-assembly at bare semiconductor surfaces: Preparation and characterization of highly organized octadecanethiolate monolayers on GaAs(001)," *J. Am. Chem. Soc.*, vol. 128, no. 15, pp. 5231–5243, 2006.

[14] R. C. Kim, P. C. M. F. Bent, R. Chen, H. Kim, and P. C. Mcintyre, "Self-assembled monolayer resist for atomic layer deposition of high- κ gate dielectrics Self-assembled monolayer resist for atomic layer deposition of HfO 2 and ZrO 2 high- □ gate dielectrics," 2004.

[15] M. Ikenaga, K. Nakamura, A. Tachibana, and K. Matsumoto, "Quantum chemical study of gas-phase reactions of trimethylaluminium and triethylaluminium with ammonia in III-V nitride semiconductor crystal growth," *J. Cryst. Growth*, vol. 237–239, no. 1–4 II, pp. 936–941, 2002.

[16] S. E. Roadman, N. Maity, J. N. Carter, and J. R. Engstrom, "Study of thin film deposition processes employing variable kinetic energy, highly collimated neutral molecular beams," *J. Vac. Sci. Technol. A Vacuum, Surfaces, Film.*, vol. 16, no. 6, p. 3423, 1998.

[17] S. Hofmann, "Practical surface analysis: state of the art and recent developments in AES, XPS, ISS and SIMS," *Surf. Interface Anal.*, vol. 9, no. 1, pp. 3–20, 1986.

[18] T. L. Barr, "Nature of the use of adventitious carbon as a binding energy standard," *J. Vac. Sci. Technol. A Vacuum, Surfaces, Film.*, vol. 13, no. 3, p. 1239, 1995.

[19] R. Alfonsetti, L. Lozzi, M. Passacantando, P. Picozzi, and S. Santucci, "XPS studies on SiOx thin films," *Appl. Surf. Sci.*, vol. 70–71, no. PART 1, pp. 222–225, 1993.

[20] P. Larson, "Journal of electron Spectroscopy and related Phenomena," vol. 4, pp. 213–218, 1974.

[21] D. A. Shirley, “High-resolution x-ray photoemission spectrum of the valence bands of gold,” *Phys. Rev. B*, vol. 5, no. 12, pp. 4709–4714, 1972.

[22] J. H. Scofield, “Hartree-Slater subshell photoionization cross-sections at 1254 and 1487 eV,” *J. Electron Spectros. Relat. Phenomena*, vol. 8, no. 2, pp. 129–137, 1976.

[23] L. T. Zhuravlev, “Concentration of hydroxyl groups on the surface of amorphous silicas,” *Langmuir*, vol. 3, no. 3, pp. 316–318, 1987.

[24] S. R. Wasserman, Y. T. Tao, and G. M. Whitesides, “Structure and reactivity of alkylsiloxane monolayers formed by reaction of alkyltrichlorosilanes on silicon substrates,” *Langmuir*, vol. 5, no. 4, pp. 1074–1087, 1989.

[25] C. H. Bartholomew, P. K. Agrawal, and J. R. Katzer, “Sulfur Poisoning of Metals,” *Adv. Catal.*, vol. 31, no. C, pp. 135–242, 1982.

[26] W. Zhang, “Wenyu Zhang’s Dissertation,” no. February, 2016.

[27] M. Foss, R. Feidenhans’l, M. Nielsen, E. Findeisen, T. Buslaps, R. L. Johnson, and F. Besenbacher, “Sulfur induced Cu4 tetramers on Cu(111),” *Surf. Sci.*, vol. 388, no. 1–3, pp. 5–14, 1997.

[28] F. Wiame, V. Maurice, and P. Marcus, “Reactivity to sulphur of clean and pre-oxidised Cu(1 1 1) surfaces,” *Surf. Sci.*, vol. 600, no. 18, pp. 3540–3543, 2006.

[29] D. R. Alfonso, “Computational Studies of Experimentally Observed Structures of Sulfur on Metal Surface ... Page 1 of 2 Computational Studies of Experimentally Observed Structures of Sulfur on Metal Surfaces Computational Studies of Experimentally Observed Structures of S,” *Text*, pp. 1–2, 2011.

[30] Y. Bu, J. W. H. Niemantsverdriet, and H. O. A. Fredriksson, “Cu Model Catalyst Dynamics and CO Oxidation Kinetics Studied by Simultaneous in Situ UV-Vis and Mass Spectroscopy,” *ACS Catal.*, vol. 6, no. 5, pp. 2867–2876, 2016.